minerals

MDPI

Article

Revisiting Albarracín Rock Art Through Multivariate pXRF Analysis of White, Black, and Red Pigments †

Pablo Martín-Ramos [1], José Antonio Cuchí-Oterino [2,*] and Manuel Bea-Martínez [3]

[1] Advanced Materials Laboratory, ETSIIAA, University of Valladolid, Avenida de Madrid 44, 34004 Palencia, Spain; pmr@uva.es
[2] Polytechnic School of Huesca, University of Zaragoza, Carretera de Cuarte s/n, 22071 Huesca, Spain
[3] Departamento de Ciencias de la Antigüedad, Facultad de Filosofía y Letras—P3A Group & Instituto Universitario de Investigación en Patrimonio y Humanidades (IPH), University of Zaragoza, C/Pedro Cerbuna 12, 50071 Zaragoza, Spain; manubea@unizar.es
* Correspondence: cuchi@unizar.es
† In memoriam of Prof. Dr. Víctor M. Orera-Clemente (20 December 1950–28 January 2020).

Abstract

Rock art in the Albarracín Cultural Park represents one of Spain's most significant concentrations of post-Paleolithic paintings, yet comprehensive chemical characterization across multiple shelters remained lacking. This study analyzes 102 pigment samples (54 white, 31 black, 17 red) from 12 shelters using portable X-ray fluorescence spectroscopy. Centered log-ratio transformation addressed compositional data constraints, enabling multivariate analyses (PCA, LDA, MANOVA) that properly account for the constant-sum constraint inherent in geochemical data. Linear discriminant analysis achieved 92.6%–100% classification accuracy for site attribution, with barium emerging as the universal discriminating element across all pigment types (Cohen's d = 4.91–9.19). Iron concentrations confirmed hematite/goethite use in red pigments, with inter-shelter variations suggesting different ochre sources. Black pigments revealed dual technologies: manganese oxides (pyrolusite) and carbon-based materials, with phosphorus enrichment in some samples consistent with possible bone-derived materials, though alternative phosphorus sources cannot be definitively excluded. This technological duality occurred within individual shelters, documenting greater complexity than previously recognized. White pigments combined substrate-derived materials with gypsum and aluminosilicate clay minerals (likely of the kaolinite group), occasionally incorporating phosphate-rich phases. The documented coexistence of compositionally distinct pigments within single shelters (whether from different raw material sources or varied preparation techniques) confirms the technical heterogeneity of Albarracín rock art and challenges assumptions about technological homogeneity in Levantine art production. This interplay between natural geological constraints and cultural technological choices underscores the need for complementary surface-sensitive techniques to fully resolve the technological repertoire of Levantine artists.

Keywords: archaeometry; chemical fingerprinting; compositional data analysis; Levantine art; multi-elemental analysis; rock shelter; schematic art; Teruel

Academic Editor: Marco Benvenuti

Received: 30 October 2025
Revised: 2 December 2025
Accepted: 16 December 2025
Published: 18 December 2025

Citation: Martín-Ramos, P.; Cuchí-Oterino, J.A.; Bea-Martínez, M. Revisiting Albarracín Rock Art Through Multivariate pXRF Analysis of White, Black, and Red Pigments. *Minerals* **2025**, *15*, 1328. https://doi.org/10.3390/min15121328

1. Introduction

The study of pigments used in the past has been the subject of numerous investigations [1] and continues to be of interest in understanding prehistoric cave art and contributing to its preservation. Rock art pigment analysis has evolved considerably in

recent decades, with scientific methodologies now integrated with aesthetic evaluations to provide comprehensive characterization of prehistoric paintings [2].

Portable X-ray fluorescence (pXRF) spectroscopy has become an established tool for in situ elemental analysis of rock art pigments, offering the critical advantage of non-destructive characterization in remote locations where sampling is prohibited or impractical. While pXRF provides exclusively elemental composition data and cannot identify mineral phases or organic components directly, its capacity to analyze multiple elements simultaneously across large sample sets makes it particularly valuable for comparative geochemical studies and site discrimination.

However, the technique's limitations [3–5] are particularly acute in the context of thin paint layers on sandstone substrates. For major elements in siliceous matrices, X-ray penetration depths on the order of 1–5 mm greatly exceed typical pigment-layer thicknesses (usually <50 μm). As a result, pXRF spectra record composite signals in which the rock substrate contributes the majority of the counts, and the pigment layer acts mainly as a thin attenuating and modulating veneer. This geometry means that elements such as Ba and the Sr-Si-Mg triad primarily trace geological variation in the *Rodeno* sandstones and related facies, and it is these substrate-derived elements that drive much of the apparent discrimination among shelters. In contrast, elements that show clear enrichment above local substrate baselines (most notably Fe in red pigments, Mn in specific black pigments, and P in some white and black samples) are more plausibly linked to deliberate pigment composition. The interpretive strategy adopted in this study, therefore, rests on treating pXRF data as joint records of geological context and technological choice rather than as pure pigment recipes.

When coupled with advanced multivariate statistical approaches that properly account for compositional data constraints and are interpreted within explicit awareness of substrate dominance, pXRF can reveal systematic patterns in raw material procurement, technological choices, and site-specific signatures that would remain obscured in smaller-scale studies. The key interpretive principle is recognizing which discriminating elements reflect pigment recipes versus geological substrate—a distinction central to the categorization framework detailed in Section 2.4.

The rock art of the Mediterranean basin represents an exceptional collection meriting such systematic geochemical investigation. In 1998, UNESCO declared the Rock Art of the Mediterranean Basin on the Iberian Peninsula (ARAMPI) a World Heritage Site, encompassing 727 rock art complexes that represent diverse styles and chronological cycles, among which the so-called Levantine Art and Schematic Art are particularly prominent. Located along the Mediterranean coastline of the Iberian Peninsula, these prehistoric rock art shelters form an exceptional ensemble, presenting ways of life from a crucial stage in human development through paintings that, by virtue of their style and subject matter, are unique. In the Albarracín area, in the *Rodeno* sandstone landscape, 23 rock art complexes are recognized as World Heritage, although many more shelters preserve some of the most significant graphic manifestations of the Levantine artistic cycle.

Traditionally, since the "unofficial" discovery of Levantine art in 1892 [6,7] with the shelters of Los Toricos del Prado del Navazo and the Cocinilla del Obispo, the Albarracín shelters have occupied a privileged position in studies of Levantine art, largely due to the exceptional representations of large bovids painted in white and black. Numerous studies have focused on the decorated shelters of Albarracín, beginning with the scientific publications of Abbé H. Breuil and his collaborators, such as J. Cabré and H. Obermaier. Later, research in the area was continued by T. Ortego, M. Almagro, and A. Beltrán. However, aside from relatively recent and somewhat systematic investigations carried out by various scholars in the area, it is important to highlight the comprehensive work of

F. Piñón [8]. Three decades later, several documentation campaigns incorporating new technologies (digital tracings, geometric documentation, etc.) have enabled a more complete and accurate record of both the shelters and the rock motifs [9–17]. The comprehensive study of the Sierra de Albarracín complexes is the main objective of the SEFORA project (Searching for the Origins of Rock Art in Aragón), which includes a specific section on pigment analysis aimed at understanding not only the technical criteria of execution but also the decorative phases.

Despite their inherent interest in understanding prehistoric technology and cultural practices, systematic chemical analyses of pigments have only become essential in Levantine art research in recent years [18–26]. In the particular case of the Albarracín area, Beltrán Martínez [27] pointed out, without citing analytical methods, the presence of iron, aluminum, and traces of copper in paintings in Santolea (Teruel), outside the area studied. He attributed the iron to ochres and hematite, the black to vegetable carbon, and the white to kaolin. Only Orera Clemente et al. [11,28] have worked on sandstones from the *Rodeno* Formation using analytical methods.

The rock art of the Sierra de Albarracín exhibits distinctive characteristics that set it apart from other Levantine art manifestations. This distinctiveness has been characterized as a heterogeneous assemblage of artistic representations in which the bulls of Albarracín bear little resemblance to other stylizations or schematizations. The large bulls of Prado del Navazo, Los Toricos, Cocinilla del Obispo, and Ceja de Piezarrodilla exhibit notable departures from typical Levantine art conventions in terms of color, size, and stylistic features [29]. Beltrán observes that "the strange animal representations of the Tío Campano shelter, or the tiny human figures of the Lázaro shelter, introduce elements so inconsistent with what is known that they will force a reconsideration of this regional nucleus of parietal graphic expression" [29]. He also points out the distinctive character of the white figures of the Sierra de Albarracín, which are naturalistic and Paleolithic in appearance [30], and which, in his view, demonstrate the enduring presence of the earliest repainted figures [29]. Compared to what can be observed in other regions with Levantine rock art, that of Albarracín constitutes such a distinct unity and such an exception in its landscape, themes, and techniques, style, pigmentation, and scale, that these artistic manifestations have become an indispensable point of reference for the study of prehistoric art.

As part of the SEFORA program, a systematic non-destructive study of the cave paintings at *Rodeno* was undertaken using portable X-ray fluorescence during the summer of 2025. The primary objective is to chemically characterize the pigments and underlying rock substrates, particularly in cases where layering or superimposition may have occurred. Beyond compositional analysis, this research aims to identify geochemical signatures that may discriminate between shelters and potentially reveal multiple painting phases within individual sites. By integrating advanced multivariate statistical approaches with high-resolution elemental data, this study seeks to elucidate both the technological knowledge of Levantine artists and the spatio-temporal complexity of painting activities across the Albarracín region. The results will provide critical insights into raw material procurement strategies, pigment preparation techniques, and the cultural practices underlying one of Europe's most enigmatic rock art traditions.

2. Materials and Methods

2.1. Studied Area and Rock Shelters

The twelve rock art shelters analyzed in this study are located within the Albarracín Cultural Park, Sierra de Albarracín, Teruel, Spain (Figure 1). These shelters represent a significant concentration of post-Paleolithic rock art, with paintings attributed primarily to the Levantine and Schematic art traditions. The shelters include: Cabras Blancas, Casa

Forestal I, Casa Forestal II, Casa Forestal V, Ceja de Piezarrodilla, Hoya de Navarejos II, Hoya de Navarejos III, Hoya de Navarejos IV, Hoya de Navarejos V, La Cocinilla del Obispo, Prado Navazo, and Tío Campano.

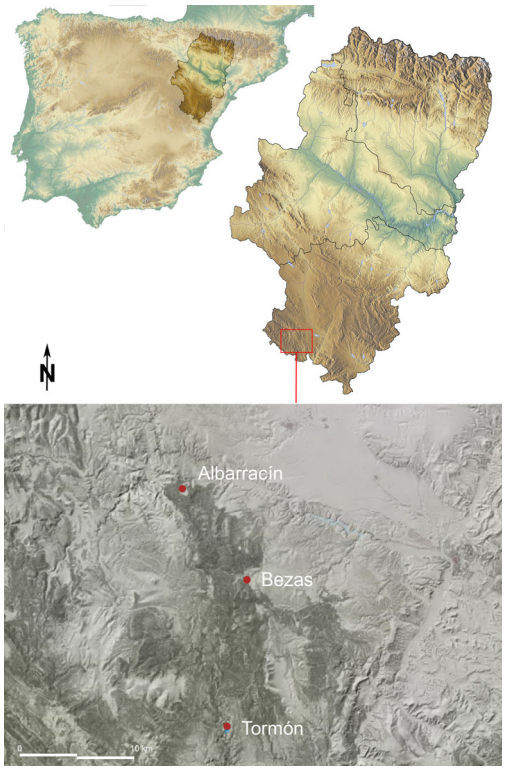

Figure 1. Map of the study area showing shelter locations.

Detailed descriptions of each shelter, including their archeological context, preserved motifs, conservation state, and specific characteristics of the analyzed paintings, are provided in the Supporting Information (Section S1). The tracings of analyzed paintings from each shelter, showing the precise location of sampling points, are presented in Figures S1–S12.

2.2. Geological Setting

Rock is the medium for cave paintings. On the one hand, pigments have evolved on and with a rock substrate that is not inert and cannot be separated for non-destructive in situ analysis. Therefore, it is necessary to adequately characterize its nature. On the other hand, at least some of the pigments are mineral substances, with minor treatment such as grinding, and are presumed to have been extracted from nearby geological resources.

All the paintings in this study are located in the *Rodeno*, a very distinctive Permo-Triassic geological landscape in the Buntsandstein facies. Its materials are mainly fluvial sandstones with abundant cross-stratification in centimeter-thick and even thinner layers deposited between the late Paleozoic and early Mesozoic.

Lithologically, the support for the paintings is reddish sandstone, classified as litharenite and formed by medium-sized, subrounded or subangular grains of quartz (45%), quartzite fragments (10%), flint (5%), and micas, quartz cement, and a sericite matrix (20%) impregnated with iron oxide (20%). Frequent parallel microstratification and local development of secondary quartz growth occur throughout. The Spanish Geological and Mining Institute (IGME) [31,32] indicates the presence of zircon ($ZrSiO_4$), rutile (TiO_2), and tourmaline ($(Na,Ca)(Al,Fe,Li)(Al,Mg,Mn)_6(BO_3)_3(Si_6O_{18})(OH,F)_4$). Iron Liesegang rings

are frequent and sometimes very abundant. In some areas, there are iron oxide concretions at the top of the section, parallel to the stratification.

De la Cruz et al. [33] identify three large sedimentary units in this formation with different source areas and different diagenetic processes. They indicate the presence of quartz, feldspars, and their clay alteration, and remains of metamorphic rocks. The association of heavy minerals in the three units is monotonous and scarce, with tourmaline, zircon, leucoxene (a mixture of titanium minerals), opaque minerals, and, in even smaller proportions, rutile. In the lower unit, they note the presence of barite and uranium minerals. In general, porosity is moderate, around 10%, which allows partial penetration of the pigments into the rock itself.

The stratigraphy is complex, and up to 16 lithostratigraphic units have been differentiated [34–37]. These units correspond to proximal braided river deposits; however, the abundance of reactivation surfaces suggests the intervention of marine tides in the reworking of the fluvial deposits. They are arranged in thick banks with predominantly cross-bedded stratification and erosion and reactivation surfaces that separate the groups of sets. The paleocurrents have elongated grooves between N-130-E and N-180-E. The predominant direction of contribution is to the S or SE. Locally, the Spanish Geological and Mining Institute [31,32] indicates the presence of caliche levels or calcimorphic soils. The tectonics are complex, dominated by large NW-SE fractures (the Calatayud-Teruel trench) and locally minor fractures that can reach metric densities. These fractures, enlarged by erosion, give rise to numerous alleys that isolate sandstone outcrops.

The landscape of the *Rodeno* is peculiar as continuous erosion by wind and water has sculpted these rocks, creating alleys, isolated monoliths, visors, shelters, taffonis, gnammas, and honeycombs [38]. The rock is destroyed by sandification and plane lift off. Locally, crusts and varnishes may appear on the rock. The presence of gypsum and calcite in efflorescence crusts in small ponds on the sandstones was noted by Benito et al. [39]. These salts, related to haloclastic processes, were not detected in the rock itself. The presence of calcium oxalates (whewellite) was identified by Raman analysis in the Ceja de Piezarrodilla shelter by Orera Clemente et al. [11].

Finally, it should be noted that there are numerous iron deposits inside the *Rodeno*, some mined in the past. To the north and east, the *Rodeno* sandstones are surrounded by more modern Jurassic and Cretaceous limestones. This latter system includes the Arenas de Utrillas formation, dating from the Aptian to Turonian ages and consisting of loose quartz sands locally rich in illite and kaolinite.

2.3. In Situ Measurements

Field measurements were conducted during July and August 2025 with the permission of the cultural authorities of the Government of Aragón and the cooperation of the Parque Cultural de Albarracín. The non-destructive characterization of pigments was performed using a portable X-ray fluorescence spectrometer model NITON XL3t GOLDD+ (ThermoFisher Scientific; Waltham, MA, USA), equipped with a 2 W miniaturized air-cooled X-ray tube (thin Ag anode in transmission geometry; 6–50 kV/200 μA max.) and a silicon geometrically optimized wide area drift detector (30 mm^2, 178 eV@MnKα). The analytical range encompasses elements between Mg and U. Measurement conditions employed Mining mode with the following parameters: light range (30 s): 8 kV, no filter; low range (30 s): 20 kV 1 Cu mil filter; main range (30 s): 38 kV, 4 Al + 1 Ti + 4 Fe mil filter; high range (30 s): 50 kV, 3 Mo + 4 Fe mil filter. Certified reference materials served as internal standards for monitoring instrument stability throughout the analytical campaign. Spectra processing was performed using NDT™ PC software v.8.5.1.

Regarding color classification and surface preparation, pigments were assigned to color categories (white, black, red) by visual assessment during fieldwork. No quantitative color measurements (spectrophotometry or CIE L*a*b* colorimetry) were acquired. Consequently, this study does not attempt to model relationships between numerical color parameters and elemental composition. Visual color categories serve as a coarse grouping variable for statistical analysis, but should not be interpreted as representing continuous colorimetric data.

No surface cleaning or preparation was performed prior to pXRF measurements to avoid any risk of damage to the painted surfaces. Measurements were acquired directly on the pigment surfaces as preserved, including any overlying biofilms, dust accumulation, or weathering patinas. While this preserves surface integrity, it means that measured compositions integrate contributions from (1) the original pigment layer, (2) the underlying rock substrate, and (3) any surface accumulations or alterations developed over millennia. The potential influence of biofilms and surface weathering products on measured compositions is acknowledged in the Discussion (Section 4.5).

A total of 102 pigment samples were analyzed across the 12 rock art shelters. White pigment samples (n = 54) were collected from nine shelters: Casa Forestal I (n = 2), Casa Forestal II (n = 4), Casa Forestal V (n = 3), Ceja de Piezarrodilla (n = 8), Hoya de Navarejos II (n = 2), Hoya de Navarejos III (n = 11), Hoya de Navarejos V (n = 1), La Cocinilla del Obispo (n = 5), and Prado Navazo (n = 18). Black, black-over-white, and white-over-black pigment samples (n = 31) were analyzed from six shelters: Cabras Blancas (n = 11), Ceja de Piezarrodilla (n = 10), Hoya de Navarejos III (n = 4), Hoya de Navarejos IV (n = 2), La Cocinilla del Obispo (n = 1), and Prado Navazo (n = 3). Red pigment samples (n = 17) were collected from five shelters: Casa Forestal II (n = 5), Hoya de Navarejos III (n = 1), Hoya de Navarejos V (n = 4), La Cocinilla del Obispo (n = 4), and Tío Campano (n = 3).

With regard to the sampling strategy, sampling was designed to capture chemical variation across preserved motifs at each shelter while maintaining comparable sampling intensity across sites. At shelters with multiple figures of the same pigment color (e.g., Prado Navazo with 18 white bovid figures), we selected representative samples distributed across the decorated panel rather than concentrating multiple analyses on single figures. This maximizes spatial coverage and prevents artificial inflation of between-group variation from repeated sampling of single motifs. Consequently, some shelter-color combinations have small sample sizes (e.g., n = 1 for Hoya de Navarejos V white, reflecting a single preserved white motif). Such locations were excluded from inferential parametric tests (ANOVA, MANOVA) requiring $n \geq 3$, following established statistical guidance. However, these samples contributed to exploratory multivariate analyses (PCA, hierarchical cluster analysis, LDA) and were validated through bootstrap resampling procedures (Section 2.5.2), which do not rely on minimum sample size assumptions.

Sampling points were systematically selected according to the painted motifs present in each shelter, with their locations indicated on the tracings of the paintings presented in the previous subsection. All analyses were performed in triplicate, with reported values representing the arithmetic mean of three independent measurements (n = 3).

Measurements were also acquired from unpainted rock surfaces adjacent to paintings at each shelter. At each shelter, three representative unpainted areas were selected on the characteristic sandstone surface, positioned as close as feasible to painted motifs but free from obvious pigment or biological colonization. Each location was measured in triplicate (three independent 2 min acquisitions), with the arithmetic mean of these nine measurements constituting the shelter-level substrate composition reported in Table S2. These substrate measurements characterize the typical local geological background to enable qualitative assessment of element enrichment in pigments.

Importantly, no explicit numerical 'background subtraction' was performed. Mathematical subtraction of substrate spectra from pigment spectra is problematic for pXRF data because: (a) substrate contribution varies with pigment layer thickness (unknown), (b) X-ray penetration depth varies by element and matrix composition, (c) subtraction can amplify noise and generate negative values incompatible with compositional data analysis. Instead, substrate data serve as interpretive reference points: elements showing similar concentrations in pigments and substrate are interpreted as primarily geological, while elements clearly enriched in pigments above substrate baselines are interpreted as plausibly anthropogenic additions.

2.4. Interpretation of Composite Signals and Element Categorization

To aid interpretation of composite pXRF signals, pigment measurements were qualitatively compared with unpainted rock measurements from each shelter (Table S2), allowing identification of elements that are clearly enriched or track substrate values. Based on these comparisons and element behavior in multivariate space, three practical categories were distinguished: (1) substrate-dominated elements (Ba, Sr, Si, Mg), primarily reflecting geological provenance and enabling site discrimination through regional geological variations; (2) pigment-informative elements (Fe in red pigments, Mn where strongly enriched above substrate, P where clearly elevated above substrate), reflecting intentional additions or selective material procurement; (3) elements with mixed or ambiguous origins (Ca, S), potentially from both intentional pigment ingredients (gypsum paints) and geological/diagenetic processes (substrate carbonates, sulfate enrichment). This categorization framework maintains statistical rigor while avoiding over-interpretation of composite signals and recognizing that large effect sizes may primarily reflect geological rather than technological variation.

2.5. Statistical Analysis

Given the compositional nature of pXRF data, where elemental concentrations are constrained to positive values that sum to a constant (typically approaching 100%), direct application of standard multivariate statistical methods can generate spurious correlations and misleading results. To address this fundamental constraint, we applied the centered log-ratio (CLR) transformation to project the data from the simplex into unconstrained Euclidean space, following established protocols for geochemical data analysis.

Prior to transformation, elements with concentrations below 0.1% were excluded from analysis, resulting in a refined dataset of 14 quantified elements (Ba, Zr, Sr, Fe, Mn, Ti, Ca, K, Al, P, Si, Cl, S, and Mg) and the balance fraction ('Bal'). The 'Bal' variable represents the instrument-estimated fraction of light elements with atomic number $Z < 12$ (e.g., C, O, Na) required to normalize the composition to 100%, and is included to satisfy the closure constraint requisite for robust compositional data analysis. Elements excluded by this abundance criterion (including As, Hg, Sn, Sb, Pb, Cu, Zn, Ni, Co, Cr, V, among others listed in Table S1) showed sporadic detection and minimal variance across samples, limiting their discriminatory value while potentially introducing noise from measurements near detection limits. This 0.1% abundance threshold prioritizes robust, high-frequency signals while suppressing noise from trace elements. All detected elements, including those below the 0.1% threshold and below-detection-limit (BDL) values, are fully reported in Table S1 to enable alternative element selection strategies in future comparative studies.

To handle below detection limit (BDL) values recorded as zeros, which prevent direct logarithmic transformation, we implemented multiplicative replacement imputation following the methodology of Martín-Fernández et al. [40]. This approach replaces zeros with a small fraction (0.00001%), a value selected to be substantially below the instrument's

practical quantification limit while maintaining numerical stability in logarithmic transformations. This imputation strategy maintains the dataset's multivariate structure critical for subsequent PCA and hierarchical cluster analysis, while minimizing information loss that would result from casewise deletion of samples containing BDL values.

Following the CLR transformation, Z-scores were calculated to standardize the transformed values, enabling cross-element comparison and facilitating the interpretation of multivariate patterns.

2.5.1. Multivariate and Univariate Statistical Procedures

Statistical analyses were performed using R v.4.5.1. Different sample inclusion criteria were applied depending on the analytical objective. For inferential statistical tests requiring balanced group comparisons (MANOVA, ANOVA), only locations with sample sizes $n \geq 3$ were included, following established recommendations for robust multivariate analysis and to ensure adequate estimation of within-group variance. For exploratory analyses aimed at maximizing chemical information utilization (Principal Components Analysis, Linear Discriminant Analysis, Hierarchical Cluster Analysis), all samples were included regardless of location or sample size. This dual-tier approach balances statistical rigor (excluding small groups from parametric tests where distributional assumptions and variance estimation require adequate sample sizes) with information maximization (retaining all samples in distribution-free exploratory analyses subsequently validated via permutation and bootstrap methods that do not assume specific distributions or require minimum group sizes).

Principal Components Analysis (PCA) was performed on the correlation matrix of the 15-compositional variable Z-scores to identify the primary axes of chemical variation. Linear Discriminant Analysis (LDA) was conducted using the MASS package v.7.3-65 to assess classification accuracy by location and identify the most discriminating elements. Hierarchical Cluster Analysis employed Ward's method with squared Euclidean distance to reveal chemical relationships and within-location diversity patterns.

For elements showing the strongest discrimination in multivariate analyses, one-way ANOVA was conducted with location as the independent variable. Post hoc comparisons employed Bonferroni correction when variances were homogeneous (Levene's test $p \geq 0.05$) or pairwise *t*-tests with Welch correction for heterogeneous variances. Effect sizes were quantified using Cohen's d for all significant pairwise comparisons.

2.5.2. Statistical Validation Procedures

To ensure robustness of findings without reliance on parametric assumptions, comprehensive validation procedures were implemented. PERMANOVA (Permutational Multivariate Analysis of Variance) with 999 permutations was performed using the vegan package to validate multivariate location differences. Bootstrap validation (1000 iterations) assessed the stability of discriminant analysis classification accuracy. Permutation tests (9999 iterations) were applied to individual ANOVA results to confirm significance without distributional assumptions. Cross-validation stability testing (5-fold, 50 repetitions) evaluated discriminant function robustness across different data subsets.

2.5.3. Interpretation of Effect Sizes in the Context of Composite Signals

The pXRF measurements integrate signals from multiple layers: (1) surface contamination and biofilm (where present, as documented at several shelters), (2) pigment layer (typically <50 μm thickness based on rock art preservation studies), and (3) underlying substrate (dominant contributor to X-ray signal due to penetration depth of 1–5 mm for major elements in the *Rodeno* sandstones). Consequently, observed effect sizes (Cohen's d, η^2)

reflect the total compositional variance driven by substrate geology, pigment composition, and their interaction, not pigment composition alone.

To assess substrate dominance explicitly, we compared mean elemental concentrations in unpainted rock surfaces (Table S2) with pigment samples (Table S1). For substrate-derived elements (particularly the Sr-Si-Mg triad and barium), pigment measurements closely track substrate baselines (e.g., Ba in pigment measurements: 0.023%–0.866% range; Ba in substrates: 0.024%–0.763% range), indicating minimal pigment-driven variance. Conversely, for elements with strong pigment signatures (Fe in red pigments, Mn in specific black pigments, P in phosphate-enriched samples), pigment concentrations substantially exceed substrate baselines, suggesting intentional addition or concentration by pigment recipes. This distinction between substrate-derived and pigment-derived variance is critical for archeological interpretation throughout the Results and Discussion.

3. Results

3.1. Multi-Elemental Analysis

A comprehensive pXRF analysis was conducted on 102 pigment samples from 12 rock art shelters in the Albarracín region, encompassing white (n = 54); black, black-over-white, and white-over-black (n = 31); and red (n = 17) pigments.

Raw elemental data for all analyzed samples, including minor elements below 0.1% concentration, are presented in Table S1. Elemental compositions of unpainted rock substrates from each shelter are provided in Table S2. The Z-scores of CLR-transformed data for the 15 compositional variables used in statistical analyses are presented in Table S3.

3.2. White Pigment Analysis

3.2.1. Multivariate Analyses (MANOVA, PCA, LDA, HCA)

MANOVA: A PCA-reduced MANOVA (using the first 5 principal components explaining 95% of the total variance) demonstrated statistically significant multivariate differences in elemental composition between locations (Wilks' Λ = 0.025, F (40,182) = 6.055, $p = 1.019 \times 10^{-17}$).

Principal component analysis: PCA extracted three components with eigenvalues greater than 1, cumulatively explaining 86.4% of the total variance (Table S4). PC1 (39.1%) was characterized by the coherent Sr-Si-Mg substrate group and Ba; PC2 (33.8%) showed strong Ca-Al-Cl loadings; and PC3 (13.5%) was dominated by Mn. Complete factor loadings are provided in Table S5. The PCA score plots (Figures 2 and 3) reveal clear clustering for Casa Forestal II, Casa Forestal V, Hoya de Navarejos II, and Prado Navazo, while Ceja de Piezarrodilla samples show notable internal heterogeneity, with samples 16–18 separating from other Ceja de Piezarrodilla samples in both PC projections.

Discriminant analysis: Linear discriminant analysis yielded eight discriminant functions for the nine location groups, all statistically significant (Table S6). Ba emerged as the primary discriminator (Function 1 correlation −0.852), followed by the coherent Sr-Si-Mg group (all −0.637). The structure matrix (Table S7) reveals that substrate-related elements dominate discrimination, while Fe and Mn show distinct patterns potentially related to pigment composition.

Classification accuracy reached 92.6% overall (Table 1), with perfect classification accuracy (100%) for seven of the nine locations. Ceja de Piezarrodilla (62.5%) and La Cocinilla del Obispo (80.0%) showed lower accuracy due to compositional overlap with other sites: three samples from Ceja de Piezarrodilla misclassified as Hoya de Navarejos III or Prado Navazo, and one sample from La Cocinilla del Obispo misclassified as Prado Navazo.

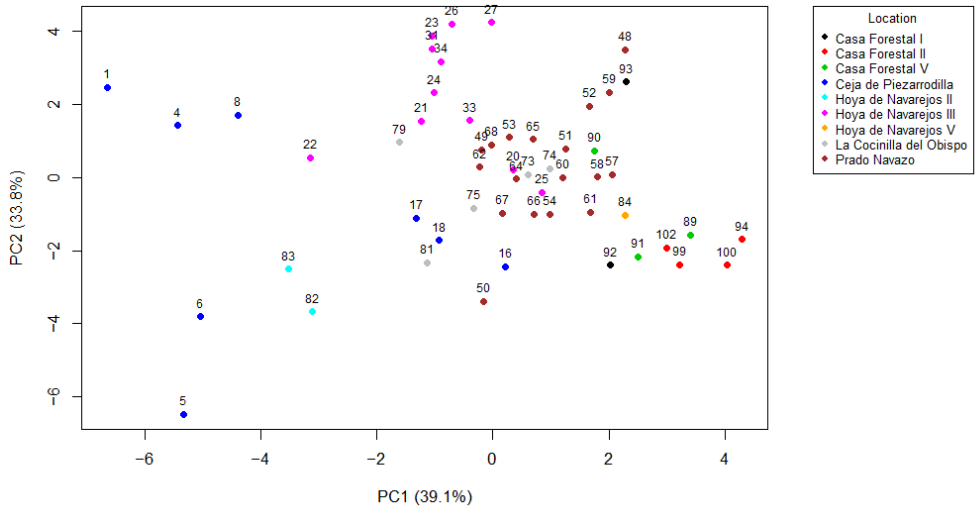

Figure 2. PCA scatter plot (PC1 vs. PC2) of white pigment samples, showing distribution by location. PC1 explains 39.1% and PC2 explains 33.8% of the total variance.

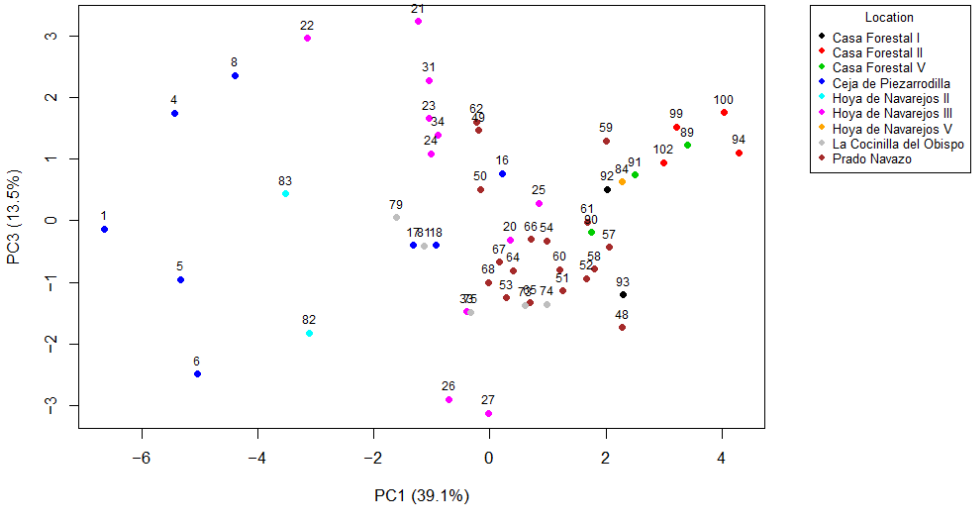

Figure 3. PCA scatter plot (PC1 vs. PC3) of white pigment samples, showing distribution by location. PC3 explains 13.5% of additional variance.

Table 1. Linear discriminant analysis classification results for white pigment samples by location.

Location	*n*	Correctly Classified	Accuracy (%)	Misclassifications
Casa Forestal I	2	2	100.0	None
Casa Forestal II	4	4	100.0	None
Casa Forestal V	3	3	100.0	None
Ceja de Piezarrodilla	8	5	62.5	Hoya de Navarejos III (2; samples 16 and 17), Prado Navazo (1; sample 18)
Hoya de Navarejos II	2	2	100.0	None
Hoya de Navarejos III	11	11	100.0	None
Hoya de Navarejos V	1	1	100.0	None
La Cocinilla del Obispo	5	4	80.0	Prado Navazo (1; sample 81)
Prado Navazo	18	18	100.0	None
TOTAL	54	50	92.6	—

Cluster analysis: Hierarchical cluster analysis (Ward's method, squared Euclidean distance) revealed varying degrees of within-locations chemical homogeneity (Figure 4, Table 2). Casa Forestal II showed the lowest chemical diversity (all samples in one cluster), while Ceja de Piezarrodilla exhibited the highest diversity (samples distributed across

four different clusters), explaining its lower LDA accuracy. Hoya de Navarejos III also showed high diversity with samples spanning four clusters despite achieving perfect LDA classification, while Prado Navazo demonstrated moderate diversity with samples distributed across four clusters.

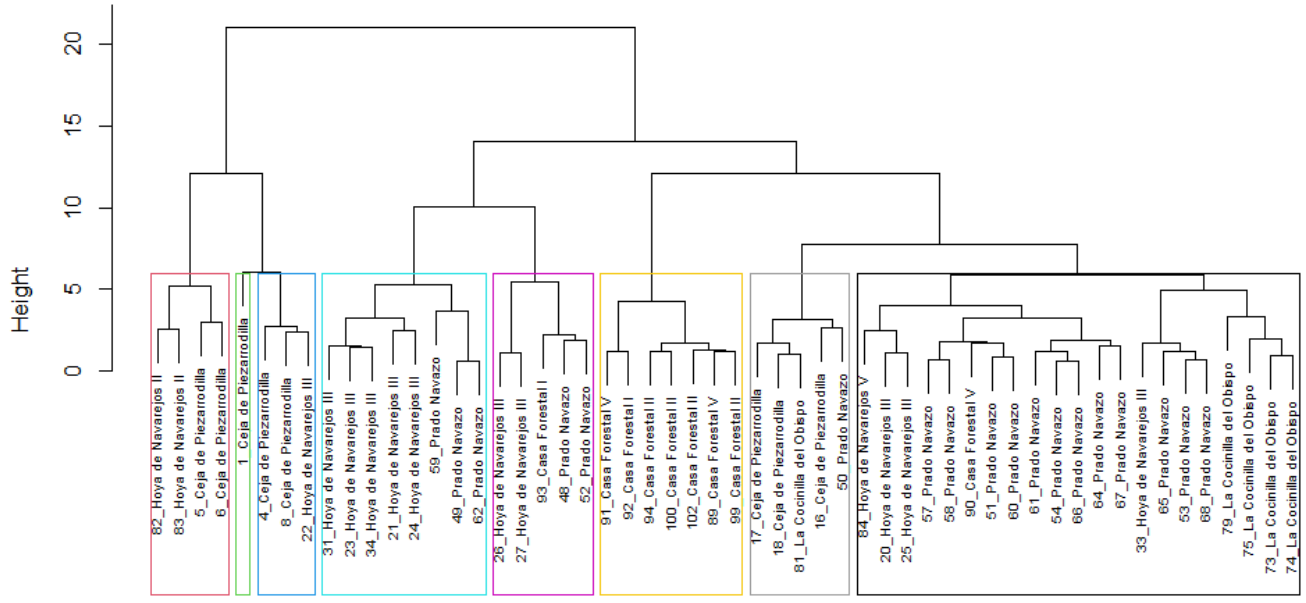

Figure 4. Hierarchical cluster dendrogram showing chemical relationships among the 54 white pigment samples. Sample labels include sample numbers and location abbreviations.

Table 2. Within-location chemical diversity of white pigment samples.

Location	*n*	Clusters (k = 8)	PC1 Range	PC2 Range	PC3 Range	Chemical Diversity
Casa Forestal I	2	2	0.28	5.01	1.71	High
Casa Forestal II	4	1	1.30	0.70	0.81	Low
Casa Forestal V	3	2	1.65	2.90	1.42	High
Ceja de Piezarrodilla	8	4	6.86	8.94	4.84	High
Hoya de Navarejos II	2	1	0.40	1.16	2.25	Low
Hoya de Navarejos III	11	4	3.98	4.65	6.35	High
Hoya de Navarejos V	1	1	0.00	0.00	0.00	Single sample
La Cocinilla del Obispo	5	2	2.60	3.30	1.53	High
Prado Navazo	18	4	2.51	6.88	3.33	Moderate

The analysis identified Casa Forestal V and Hoya de Navarejos V as the most chemically similar locations (centroid distance = 1.46 units), suggesting shared substrate characteristics or geological similarities. La Cocinilla del Obispo and Prado Navazo also showed strong chemical affinity (distance = 2.05 units). The complete distance matrix (Table S8) revealed that Casa Forestal locations maintained relatively close chemical relationships, with Casa Forestal II and Casa Forestal V showing the strongest affinity among the Casa Forestal group (distance = 1.73 units). The three Hoya de Navarejos locations (II, III, and V) displayed varying chemical relationships, with Hoya de Navarejos V showing closer affinity to Casa Forestal V than to other Hoya de Navarejos locations. In contrast, Hoya de Navarejos II and Casa Forestal II showed the greatest chemical differences (distance = 7.84 units), indicating distinct geological or pigment signatures.

Two samples from Ceja de Piezarrodilla (samples 1 and 5) were identified as chemical outliers, with PC z-scores exceeding 2.5 standard deviations from the mean. Sample 1 showed (PC1, PC2, PC3) z-scores of (−2.74, 1.10, −0.09), while sample 5 exhibited (PC1, PC2, PC3) z-scores of (−2.20, −2.87, −0.67). These outliers contribute to

the high chemical diversity observed within Ceja de Piezarrodilla (see Section 4.3 for archeological interpretation).

3.2.2. Individual Element Analysis

Statistical analysis of the five most discriminating elements (Table S9) was performed using the filtered dataset (n = 49 from 6 locations) for valid statistical inference. The eta-squared values (η^2) for all five elements indicate extremely large effect sizes: Ba exhibited the highest variance explained (η^2 = 0.708), followed by the coherent Sr-Si-Mg group (η^2 = 0.579 for all three elements, reflecting common geological substrate characteristics), and Fe (η^2 = 0.551, representing a distinct pattern of variation).

Location-specific chemical signatures (Table S10) revealed distinct chemical profiles for each location: Prado Navazo showed the highest Ba and Sr-Si-Mg concentrations; Casa Forestal V exhibited elevated Fe concentrations and moderate Sr-Si-Mg levels; and Ceja de Piezarrodilla and Hoya de Navarejos III showed depleted Sr-Si-Mg levels. La Cocinilla del Obispo and Casa Forestal II showed intermediate concentrations across most elements, with La Cocinilla del Obispo exhibiting the lowest Fe concentrations.

The post hoc pairwise comparisons (Table S11) yielded very large effect sizes, with Cohen's d ranging from 2.87 (Fe: La Cocinilla del Obispo vs. Casa Forestal II) to 4.91 (Sr-Si-Mg: La Cocinilla del Obispo vs. Casa Forestal II) and 4.22 (Ba: Ceja de Piezarrodilla vs. Casa Forestal II).

These large effect sizes likely reflect the composite nature of pXRF measurements, capturing both pigment and substrate signals. The dominance of substrate-derived elements (Ba, Sr-Si-Mg) in driving these effect sizes suggests that geological variation between shelters, rather than pigment recipes alone, underlies much of the observed discrimination.

3.2.3. Statistical Validation

Comprehensive validation confirmed the robustness of observed differences between locations without reliance on parametric assumptions (Table 3).

Table 3. Advanced statistical validation summary for white pigment samples.

Method	Statistic	*p*-Value	CI 95	Interpretation
PERMANOVA global	R^2 = 0.4932	0.001	–	Large effect
Bootstrap LDA	Accuracy = 96.5%	–	90.7%–100.0%	Robust classification
Cross-validation LDA	Accuracy = 72.7%	–	64.3%–80.8%	Stable generalization

PERMANOVA (999 permutations) demonstrated a large multivariate effect (R^2 = 0.493, p = 0.001), indicating that 49.3% of the total variance in elemental composition can be attributed to location differences.

Bootstrap validation (1000 iterations) yielded a mean accuracy of 96.5% (95% CI: 90.7%–100.0%), very similar to the original classification accuracy of 92.6%, indicating excellent stability and minimal overfitting in the discriminant model.

Cross-validation analysis (5-fold, 50 repetitions) achieved 72.7% accuracy (95% CI: 64.3%–80.8%). While showing a more substantial decrease from the original accuracy, this still represents strong predictive performance and demonstrates that the discriminant model maintains robust predictive power on unseen data.

Permutation tests (9999 iterations) for individual element ANOVAs confirmed the parametric results without distributional assumptions. All five discriminating elements (Ba, Sr, Si, Mg, Fe) maintained extremely high statistical significance with permutation p-values ≤ 0.0001, validating the exceptional discriminatory power of these elements.

3.3. Black, Black-over-White, and White-over-Black Pigment Analysis

3.3.1. Multivariate Analyses (MANOVA, PCA, LDA, HCA)

MANOVA: A PCA-reduced MANOVA (5 components, 95.6% variance) demonstrated statistically significant multivariate differences in elemental composition between locations (Wilks' $\Lambda = 0.018$, F (25,80) = 16.428, $p = 1.589 \times 10^{-10}$).

Principal component analysis: PCA extracted four components with eigenvalues greater than 1, cumulatively explaining 90.6% of the total variance (Table S12). PC1 (58.9%) showed opposing patterns between Ba-Sr-Mn-Si-Mg (negative) and Al-Zr-P-Cl-S (positive); PC2 (12.3%) captured K-Al-Cl versus Zr-P-S contrasts; PC3 (10.4%) was dominated by Ti and Ca; and PC4 (9.0%) reflected the Sr-Si-Mg substrate group. Complete factor loadings are presented in Table S13.

The PCA score plots (Figures 5 and 6) show Ceja de Piezarrodilla clustering distinctly, with samples 14 and 15 emerging as notable outliers with high PC3 values.

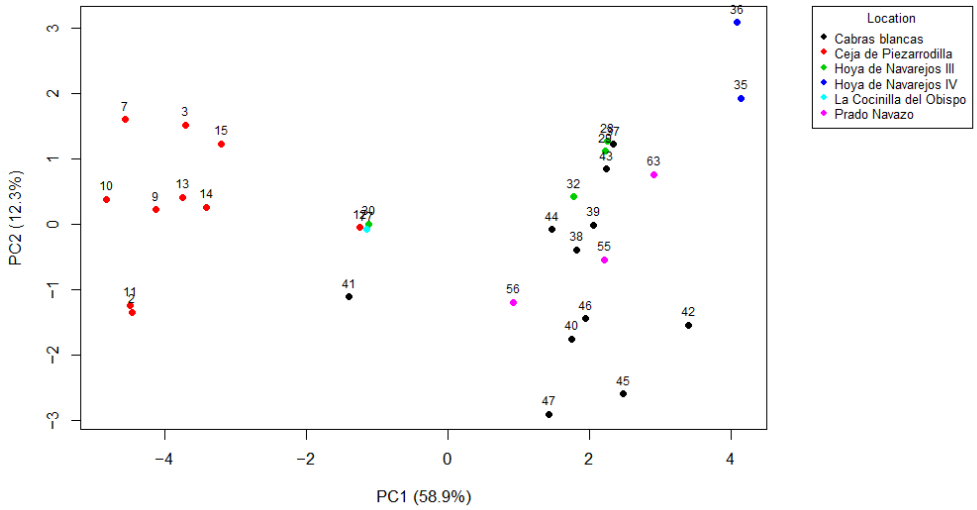

Figure 5. PCA scatter plot (PC1 vs. PC2) of black, black-over-white, and white-over-black pigment samples, showing distribution by location. PC1 explains 58.9% and PC2 explains 12.3% of the total variance.

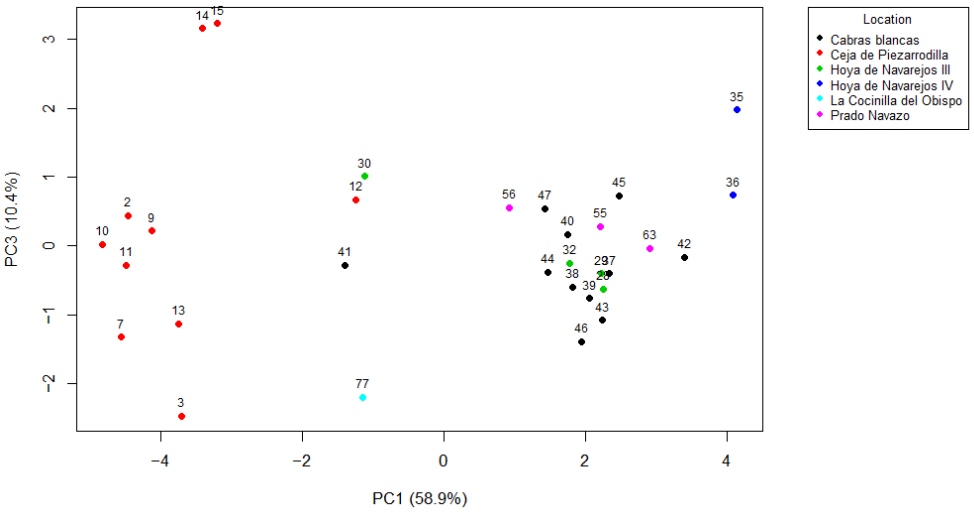

Figure 6. PCA scatter plot (PC1 vs. PC3) of black, black-over-white, and white-over-black pigment samples, showing distribution by location. PC3 explains 10.4% of additional variance.

Discriminant analysis: LDA yielded perfect classification accuracy (100.0%, Table 4) with five discriminant functions (Tables S14). Barium dominated Function 1 (correlation −0.970),

followed by the Sr-Si-Mg group (−0.799). Function 2 captured Mn (0.565) and K (0.458) variation. Structure matrix coefficients are presented in Table S15. Cross-validation accuracy was 77.5%, indicating some degree of overfitting but still demonstrating strong discriminative capability.

Table 4. Linear discriminant analysis classification results for black, black-over-white, and white-over-black pigment samples by location.

Location	*n*	Correctly Classified	Accuracy (%)	Misclassifications
Cabras Blancas	11	11	100.0	None
Ceja de Piezarrodilla	10	10	100.0	None
Hoya de Navarejos III	4	4	100.0	None
Hoya de Navarejos IV	2	2	100.0	None
La Cocinilla del Obispo	1	1	100.0	None
Prado Navazo	3	3	100.0	None
TOTAL	31	31	100.0	---

Cluster analysis: HCA revealed varying within-location chemical homogeneity (Figure 7). Ceja de Piezarrodilla demonstrated internal chemical heterogeneity at lower hierarchical levels but maintained overall coherence with all samples grouping under a common major branch. In contrast, Cabras Blancas showed true chemical scattering, with samples distributed across multiple major hierarchical branches rather than forming a coherent location-based cluster. Hoya de Navarejos IV exhibited the tightest clustering consistency across all hierarchical levels.

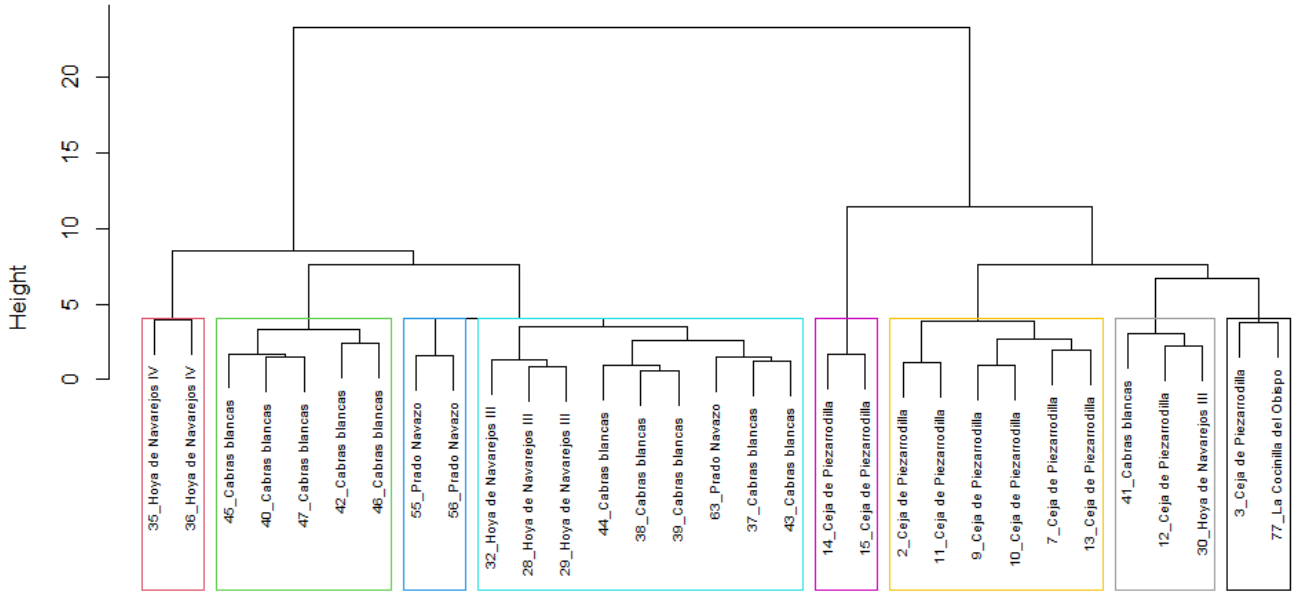

Figure 7. Hierarchical cluster dendrogram showing chemical relationships among the 31 black, black-over-white, and white-over-black pigment samples. Sample labels include sample numbers and location abbreviations.

Quantitative assessment of within-location chemical diversity (Table 5) revealed distinct patterns. Ceja de Piezarrodilla exhibited the highest chemical diversity (PC1 range 3.59, PC2 range 2.95, PC3 range 5.70) and distribution across four different clusters at k = 8 analysis. Cabras Blancas showed moderate diversity metrics (PC1 range 4.80, PC2 range 4.13) with samples distributed across three clusters, though this moderate quantitative diversity masks the more complex scattering pattern revealed by HCA. Hoya de Navarejos III displayed high diversity with substantial PC ranges (PC3 range 1.63) across

two clusters, while Prado Navazo demonstrated the most constrained chemical variation, with all samples forming a single tight group. Hoya de Navarejos IV showed the lowest diversity metrics (PC1 range 0.06, PC2 range 1.16), consistent with its cohesive clustering behavior.

Table 5. Within-location chemical diversity of black, black-over-white, and white-over-black pigment samples.

Location	*n*	Clusters (k = 8)	PC1 Range	PC2 Range	PC3 Range	Chemical Diversity
Cabras Blancas	11	3	4.80	4.13	2.12	Moderate
Ceja de Piezarrodilla	10	4	3.59	2.95	5.70	High
Hoya de Navarejos III	4	2	3.38	1.27	1.63	High
Hoya de Navarejos IV	2	2	0.06	1.16	1.24	High
La Cocinilla del Obispo	1	1	0.00	0.00	0.00	Single sample
Prado Navazo	3	1	1.99	1.95	0.59	Low

The most chemically similar locations were Prado Navazo and Cabras Blancas (centroid distance 1.61 units). The complete distance matrix (Table S16) revealed that Hoya de Navarejos III also showed relatively close chemical affinity to both Cabras Blancas and Prado Navazo. In contrast, Hoya de Navarejos IV and Ceja de Piezarrodilla showed the greatest chemical differences (distance = 8.31 units). Samples 14 and 15 from Ceja de Piezarrodilla were identified as chemical outliers (PC3 z-scores of 2.53 and 2.59, respectively), corresponding to a distinct preservation zone within the shelter, and are discussed further in Section 4.5 regarding their taphonomic significance.

3.3.2. Individual Element Analysis

Analysis of the five most discriminating elements (Table S17) used the filtered dataset (locations with $n \geq 3$) for valid statistical inference. All elements showed large effect sizes: Ba ($\eta^2 = 0.929$, explaining 93% of the variance), the coherent Zr-P-S group ($\eta^2 = 0.739$), and Mn ($\eta^2 = 0.728$).

Concerning location-specific chemical signatures (Table S18), Hoya de Navarejos III showed the highest Ba and extraordinarily elevated Mn, with depleted Zr-P-S; Ceja de Piezarrodilla showed the opposite pattern (elevated Zr-P-S, depleted Ba-Mn); Cabras Blancas showed moderately elevated Zr-P-S concentrations with depleted Ba and the lowest Mn levels; and Prado Navazo exhibited intermediate levels.

Post hoc comparisons (Table S19) revealed numerous significant pairwise differences with extraordinarily large effect sizes: Ba between Ceja and Prado Navazo (Cohen's d = 9.08), Mn between Ceja and Prado Navazo (d = 7.50), and Zr-P-S between Ceja and Prado Navazo (d = 3.56).

These extreme effect sizes reflect combined substrate geology and pigment composition influences. The Mn pattern is particularly significant archeologically: high Mn (>0.3%) indicates manganese oxide pigments, while Mn-absent samples with elevated P suggest carbon-based blacks possibly incorporating bone-derived materials.

3.3.3. Statistical Validation

Validation analyses confirmed robust compositional differences (Table 6). PERMANOVA demonstrated a very large effect size ($R^2 = 0.587$, $p = 0.001$). Bootstrap validation of the discriminant analysis yielded 99.8% accuracy (95% CI: 96.8%–100.0%), and cross-validation analysis achieved 77.5% (95% CI: 68.5%–86.6%). Permutation tests confirmed all five discriminating elements (Ba, Zr, P, S, Mn) at $p < 0.0001$.

Table 6. Advanced statistical validation summary for black, black-over-white, and white-over-black pigment samples.

Method	Statistic	*p*-Value	95% CI	Interpretation
PERMANOVA global	$R^2 = 0.5866$	0.001	–	Very large effect
Bootstrap LDA	Accuracy = 99.8%	–	96.8%–100.0%	Robust classification
Cross-validation LDA	Accuracy = 77.5%	–	68.5%–86.6%	Stable generalization

3.4. Red Pigment Analysis

3.4.1. Multivariate Analyses (MANOVA, PCA, LDA, HCA)

MANOVA: PCA-reduced MANOVA showed extremely strong evidence for location-based compositional differences (Wilks' $\Lambda = 0.001$, $F(20,27) = 19.937$, $p = 1.276 \times 10^{-7}$).

Principal component analysis: PCA extracted three components explaining 86.7% of the total variance (Tables S20 and S21). PC1 showed strong Al-Cl-Ca contributions; PC2 captured the Sr-Si-Mg substrate group (0.406) contrasted with Zr-P-S (−0.333); and PC3 reflected K-Mn variation.

The PCA score plots (Figures 8 and 9) show Casa Forestal II forming a clear and tight cluster, while sample 19 from Hoya de Navarejos III emerges as a significant outlier. Tío Campano samples show high within-location variability.

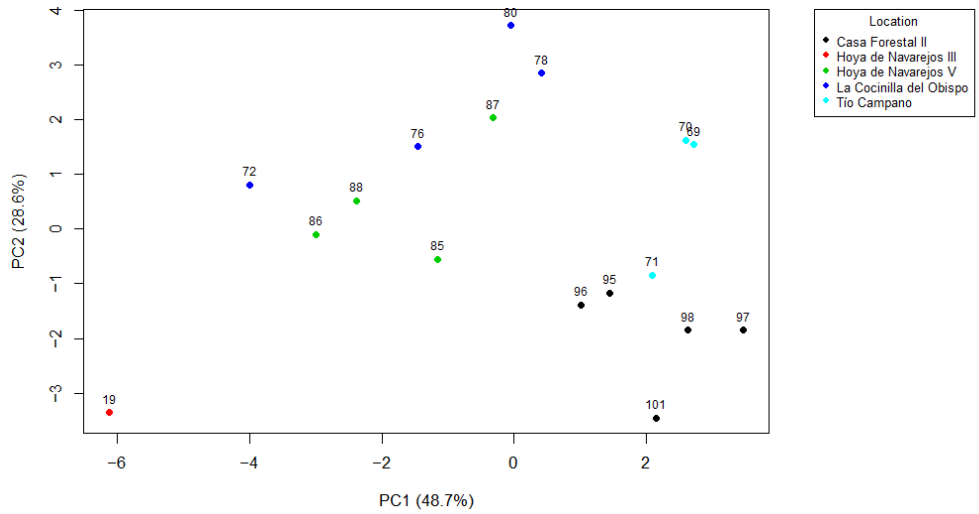

Figure 8. PCA scatter plot (PC1 vs. PC2) of red pigment samples showing distribution by location.

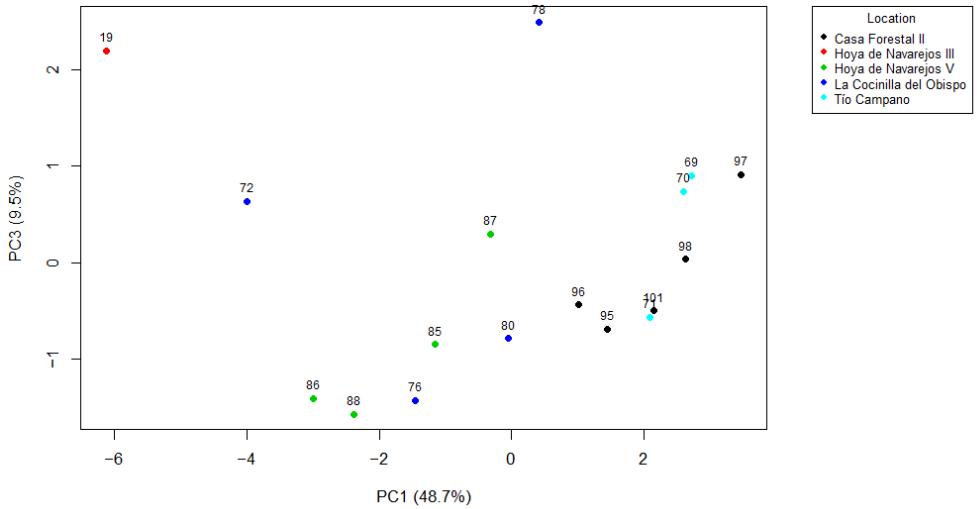

Figure 9. PCA scatter plot (PC1 vs. PC3) of red pigment samples showing distribution by location.

Discriminant analysis: LDA achieved perfect classification (100%, 17/17 correct; Table 7) with four discriminant functions (Table S22). Function 1 was driven by Ba (−0.802) and Fe (0.823); Function 2 by Sr-Si-Mg (0.846). Structure coefficients are detailed in Table S23.

Table 7. Linear discriminant analysis classification results for red pigment samples by location.

Location	*n*	Correctly Classified	Accuracy (%)	Misclassifications
Casa Forestal II	5	5	100.0	None
Hoya de Navarejos III	1	1	100.0	None
Hoya de Navarejos V	4	4	100.0	None
La Cocinilla del Obispo	4	4	100.0	None
Tío Campano	3	3	100.0	None
TOTAL	17	17	100.0	None

Cluster analysis: HCA revealed complex chemical relationships between samples (Figure 10). The analysis showed mixed clustering patterns, with samples from different locations sometimes grouping together and samples from the same location occasionally appearing in separate clusters. This suggests overlapping chemical signatures between some locations (La Cocinilla del Obispo, Hoya de Navarejos III, and Hoya de Navarejos V).

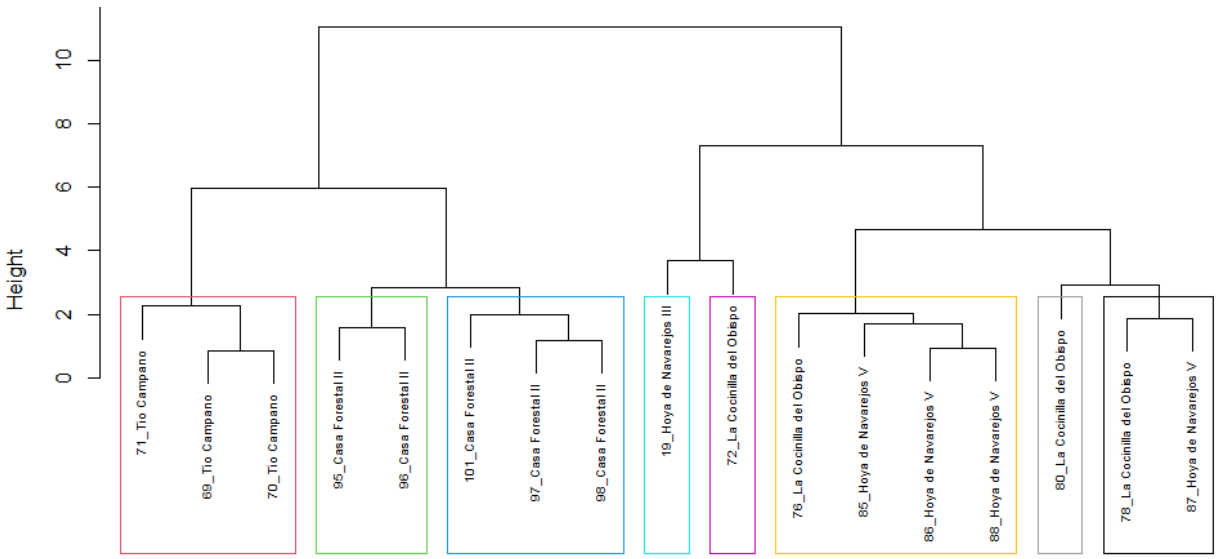

Figure 10. Hierarchical cluster dendrogram showing chemical relationships among the 17 red pigment samples.

La Cocinilla del Obispo exhibited the highest chemical diversity (Table 8), with samples distributed across four different clusters and the largest PC1 range (4.41). In contrast, Tío Campano showed the lowest chemical diversity among multi-sample locations, with all samples clustering closely together despite moderate PC2 range variations. Hoya de Navarejos V demonstrated high diversity with samples distributed across two clusters each. Casa Forestal II showed some internal chemical heterogeneity, with samples forming subgroups before clustering together as location-based units.

The cluster analysis identified La Cocinilla del Obispo and Hoya de Navarejos V as the most chemically similar locations (centroid distance = 1.62 units, Table S24), while Tío Campano and Hoya de Navarejos III were the most different (distance = 8.07). No extreme chemical outliers were detected (all $|z| < 2.5$).

Table 8. Within-location chemical diversity of red pigment samples.

Location	*n*	Clusters (k = 8)	PC1 Range	PC2 Range	PC3 Range	Chemical Diversity
Casa Forestal II	5	2	2.46	2.28	1.60	Moderate
Hoya de Navarejos III	1	1	0.00	0.00	0.00	Single sample
Hoya de Navarejos V	4	2	2.68	2.58	1.86	High
La Cocinilla del Obispo	4	4	4.41	2.92	3.91	High
Tío Campano	3	1	0.63	2.47	1.47	Low

3.4.2. Individual Element Analysis

Analysis of the five most discriminating elements (Table S25) used the filtered dataset (locations with $n \geq 3$). All elements showed extremely large effect sizes: Fe ($\eta^2 = 0.863$), Sr-Si-Mg ($\eta^2 = 0.833$), and Ba ($\eta^2 = 0.799$).

With regard to location-specific chemical signatures (Table S26), Casa Forestal II showed extraordinarily elevated Fe (the highest of all locations) with depleted Ba; Hoya de Navarejos V demonstrated the highest Sr-Si-Mg, with moderate Fe and depleted Ba; La Cocinilla del Obispo had the highest Ba, with moderate Fe and intermediate Sr-Si-Mg; and Tío Campano showed depleted Sr-Si-Mg, with moderate Fe and low Ba.

Post hoc comparisons (Table S27) revealed the largest effect size in the entire study for Ba between Tío Campano and Hoya de Navarejos V (Cohen's d = 9.19); Fe comparisons showed Casa Forestal II significantly enriched versus other locations (d = 5.75 vs. Tío Campano); and the highest concentrations for Sr-Si-Mg at Hoya de Navarejos V contrasted most strongly against Casa Forestal II (d = 4.87).

The Fe enrichment pattern is archeologically significant: consistent Fe elevation above substrate baselines confirms deliberate addition of iron oxide pigments (hematite/goethite), with inter-shelter variation suggesting different ochre sources.

3.4.3. Statistical Validation

Validation confirmed robust differences (Table 9). PERMANOVA showed a very large effect ($R^2 = 0.676$, $p = 0.001$), indicating 67.6% of the variance was attributable to location. Bootstrap validation achieved 99.4% accuracy (95% CI: 94.1–100.0%). Cross-validation yielded 69.4% (95% CI: 52.0%–82.7%). Permutation tests confirmed all discriminating elements at $p < 0.002$.

Table 9. Advanced statistical validation summary for red pigment samples.

Method	Statistic	*p*-Value	CI 95	Interpretation
PERMANOVA global	$R^2 = 0.6759$	0.001	–	Very large effect
Bootstrap LDA	Accuracy = 99.4%	–	94.1%–100.0%	Robust classification
Cross-validation LDA	Accuracy = 69.4%	–	52.0%–82.7%	Stable generalization

4. Discussion

This Discussion synthesizes the multivariate and univariate patterns documented in the Results through the lens of archeological and technological questions. The following subsections are organized around five interpretive themes: (4.1) geochemical interpretation of raw pigment compositions and their implications for material selection; (4.2) universal and pigment-specific discriminating elements and what they reveal about geological vs. cultural factors controlling compositional variation; (4.3) shelter-specific signatures and within-shelter heterogeneity as evidence for multiple painting episodes and technological complexity; (4.4) insights into pigment technology and raw material procurement; (4.5) methodological considerations, limitations, and future directions; and (4.6) archaeological and technological implications.

Figure 11 provides an integrative visual summary of the main findings, synthesizing the key discriminating elements by pigment type, the distinction between substrate-dominated and pigment-informative elements, and the inferred material components. Readers seeking a rapid overview should consult this figure before proceeding to the detailed subsections.

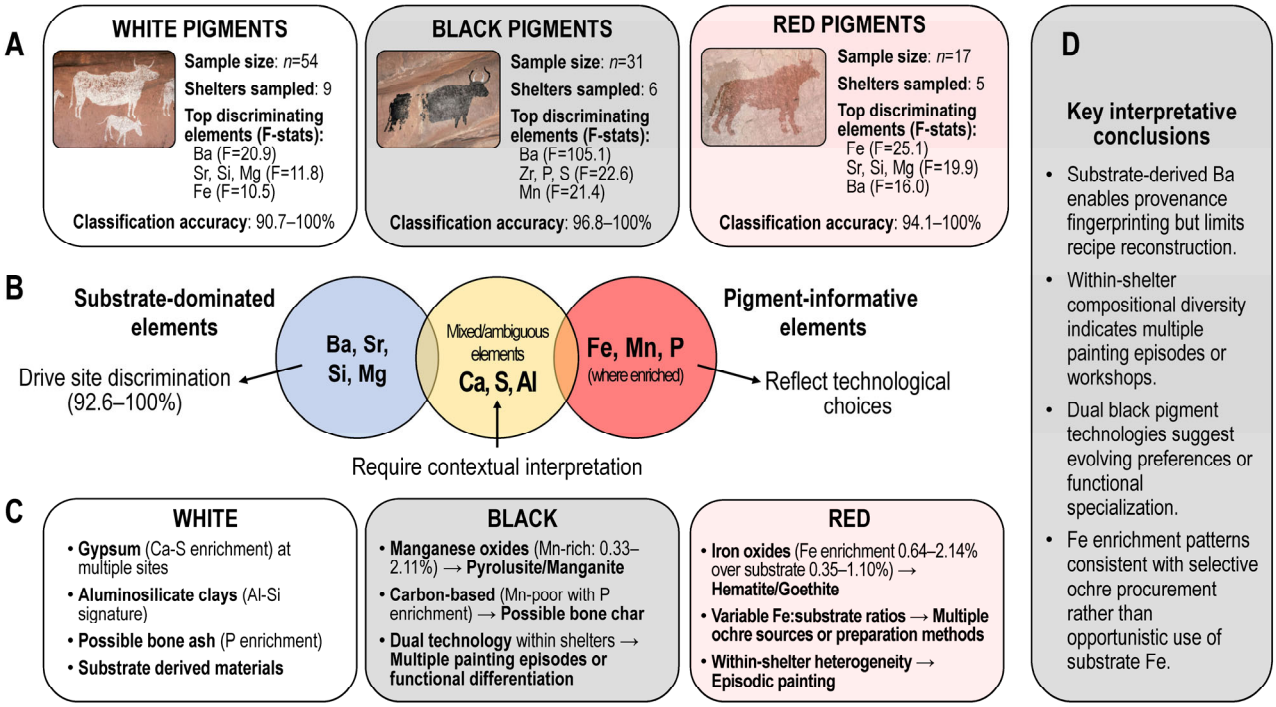

Figure 11. Integrative summary of pXRF analysis of 102 pigment samples from 12 Albarracín shelters. The schematic synthesizes: (**A**) sample distribution and classification performance by pigment type; (**B**) categorization of elements by primary origin—substrate-dominated elements (Ba, Sr, Si, Mg) drive site discrimination through geological variation while pigment-informative elements (Fe, Mn, P where enriched) reflect technological choices; (**C**) inferred material components for each pigment type based on elemental enrichment patterns; (**D**) archeological implications emphasizing that within-shelter heterogeneity documents multiple painting episodes or diverse technological traditions.

4.1. Geochemical Interpretation of Pigment Compositions

The elemental data from pXRF, prior to any transformation or statistical treatment, provide a foundational understanding of the materials present in pigmented rock surfaces at Albarracín. However, critical interpretation requires acknowledging that these measurements capture composite signals integrating substrate contribution (dominant, due to pXRF penetration depth of 1–5 mm exceeding pigment thickness of <50 μm by orders of magnitude) with genuine pigment composition. By comparing the pigment compositions (Table S1) with those of the underlying rock substrates of the shelters (Table S2), we identify elements showing clear enrichment in pigments relative to substrate baselines (signatures consistent with intentional addition or mineral selection).

Potential pigment materials are proposed based on key elemental indicators: Fe enrichment for iron oxides; Mn enrichment for manganese oxide minerals; P enrichment for phosphate-rich components potentially including bone-derived materials; Al-Si associations for aluminosilicate clay mineral phases (likely of the kaolinite group, though Si/Al ratios exceed pure kaolinite stoichiometry due to quartz substrate contribution); and Ca-S covariation for gypsum. Elements tracking substrate levels closely (particularly Ba,

Sr-Si-Mg triad, Ti) are interpreted as primarily geological in origin, enabling robust site discrimination but limiting direct 'recipe' interpretation.

These interpretations remain necessarily tentative, as pXRF provides elemental composition but cannot definitively identify crystalline phases or distinguish between mineralogically distinct materials with similar elemental ratios. Mineralogical confirmation requires complementary techniques such as X-ray diffraction or Raman spectroscopy (see Section 4.5).

Relationship between visual color and inferred composition: Although no quantitative colorimetric measurements were acquired, the visual color categories correspond logically to the elemental patterns observed. Red pigments show systematic Fe enrichment consistent with iron oxide chromophores (hematite/goethite); inter-shelter Fe variability (0.64%–2.14%) likely corresponds to perceptible color differences, with higher Fe concentrations typically producing deeper, more saturated reds. Black pigments divide into Mn-enriched samples (consistent with dark manganese oxides, pyrolusite/manganite) and Mn-poor samples (consistent with carbon-based blacks, whether charcoal or bone char, both producing deep blacks through light absorption rather than mineral pigmentation). White pigments show Ca-S-Al-Si associations consistent with gypsum and aluminosilicate clay minerals (white to cream-colored depending on iron impurity content). Quantitative colorimetric analysis combined with mineralogical identification represents an important future research direction for establishing precise color-composition relationships and detecting subtle within-category hue variations.

Ceja de Piezarrodilla: The paintings at this shelter are characterized by complex recipes and layering. Most black and all black-over-white samples show high Mn (0.33%–2.11%) relative to the substrate (<LOD), supporting the use of manganese oxides like pyrolusite as chromophores. In blacks lacking Mn presence (samples 14 and 15), the use of teruelite —a rare, ferroan variety of dolomite known for its high Fe content (approximately 10% iron substitution in the magnesium site) and characteristic dark brown to black coloration— may be considered (Mg contents of ca. 0.4% in the paintings vs. <LOD in the rock substrate and the rest of the samples), although carbon-based materials like charcoal cannot be ruled out, as they are not detectable by XRF. P concentrations (0.14–1.01%) exceed substrate levels (<LOD) in several instances, indicating the use of hydroxyapatite ($Ca_5(PO_4)_3(OH)$), likely from bone. Al and Si levels (up to 3.19% and 36.44%, respectively) suggest aluminosilicate clay mineral binders, likely of the kaolinite group, with clear enrichments over substrate (Al 1.63%, Si 13.83%) indicating deliberate addition, while high Ca and S contents largely track the substrate (mean S content in paintings 8.95% vs. 9.09% in substrate), pointing to gypsum from geological sources rather than recipes. These findings align with previous reports by Orera Clemente et al. [11], who identified an anhydrite-gypsum crust associated with a calcite flowstone at this site. Their scanning electron microscopy-energy dispersive X-ray (SEM-EDX) analyses confirmed that black pigments contained manganese oxides, presumably pyrolusite and/or manganite, with additional presence of charcoal and iron oxides (perhaps magnetite, Fe_3O_4).

Hoya de Navarejos II, III, IV, and V: The shelters at Hoya de Navarejos share a common materials base. In Hoya de Navarejos III, the white, pale red, and gray pigments are dominated by Ca (~17.35%) minerals. The white pigments show dramatic enrichment in S (mean 5.06% vs. 1.02% in rock substrate), confirming that gypsum was the principal white component. The subtle red and gray tones appear to be achieved by adding small quantities of iron oxides (hematite) and manganese oxides (pyrolusite), respectively. Black pigments at this shelter vary from Mn-rich (2.11%), indicative of pyrolusite, to Mn-absent (<LOD) with P (0.06–0.29%), suggesting bone char or charcoal. The samples from Hoya de Navarejos IV and V, though fewer, fit this pattern. The red pigments from shelter V are

defined by their Fe content (mean 1.2%), an enrichment over the substrate rock (0.96%), supporting their classification as hematite-rich ochres.

Cabras Blancas: The pigment samples from Cabras Blancas, all classified as white-over-black, are remarkably homogeneous and geochemically distinct from their substrate. The substrate here is calcareous (17.82% Ca), yet the white pigment layer is significantly enriched in Ca to an average of 23.26%. This enrichment, coupled with higher S content, indicates gypsum as a primary material. The consistent presence of low but detectable Si (~3.7%) and Al (~1.1%) suggests an aluminosilicate clay mineral component, possibly of the kaolinite group, used as a binder or extender in the gypsum paste. However, the observed Si/Al ratio (~3.4) substantially exceeds the stoichiometric ratio for pure kaolinite (~1.18 by weight), indicating significant excess silica from the quartz-rich *Rodeno* sandstone substrate. This exemplifies the challenge of mineral identification from pXRF elemental ratios alone: while the Al-Si association is consistent with clay minerals, the quantitative ratios reflect mixed pigment-substrate signals rather than pure mineral composition. The low P (0–0.023%) content and absence of Mn imply carbon-based blacks beneath (i.e., charcoal), not bone char. These results correspond with findings by Orera Clemente et al. [28], who used Raman spectroscopy and SEM-EDX to conclude that the pigment employed for the white paintings was gypsum. Regarding the black background, they noted that —based on SEM-EDX data— the composition of the black patina on which the paintings were made could be associated with the use of charcoal, although a biological origin could not be ruled out.

Prado Navazo: This shelter stands out for its extensive use of phosphate-based white: elevated P (mean ~0.45%) in conjunction with Ca strongly suggests the use of hydroxyapatite, likely in the form of calcined bone (bone ash), which would have been systematically mixed with a clay mineral (aluminosilicates consistent with kaolinite-group minerals, inferred from Si and Al) base and, in some samples, with gypsum—evidenced by significant Ca and S levels (up to 5.55%). However, low S contents (0.62–0.641%) in other white samples indicate either variability in recipes or substrate influence. The black pigments are less distinct chemically, with a composition largely mirroring the associated whites but with a slight increase in Ti, possibly indicating the use of Ti-bearing minerals or a different clay source. These could be charcoal-based, except for sample 55, in which the Mg content (0.54%) would be compatible with the use of teruelite as a chromophore.

Tío Campano: The three red samples from Tío Campano provide a clear signature for iron-based ochre. They possess the highest mean Fe concentration (2.14%) across all analyzed shelters, enriched over substrate (1.10%). This iron enrichment, combined with significant levels of Si (mean 9.78%) and Al (mean 2.36%), is highly characteristic of ferruginous clay, entirely consistent with the use of local Keuper system materials (hematite mixed with kaolinite-group clay minerals) for creating red pigments. The presence of Ca and S (1.07% in paints vs. 0.21% in substrate) suggests that gypsum may have been mixed in, perhaps to adjust the paint's consistency or hue.

La Cocinilla del Obispo: The white and pale red pigments are again primarily composed of Ca and S, consistent with a gypsum base, with red shades likely achieved by adding small amounts of iron oxides (e.g., Keuper clays with hematite). Notably, sample 80 is also rich in Ti (0.22%) and K (1.22%), suggesting the use of a different, perhaps more micaceous or feldspar-rich, clay source compared to other sites. The single black sample (77) is distinguished by its elevated Mn (0.56%), supporting the interpretation of a manganese oxide pigment (pyrolusite), which appears to have been mixed into a gypsum paste, given the high Ca and S content.

Casa Forestal I, II, and V: The rock substrate at shelters I and II is Ca-rich (14.25%–18.40%), differing in Si content (11.15% and 5.56%, respectively), while at shelter V it is Ca-poor

(0.32%) and Si-rich (41.31%), necessitating separate analysis of the white pigments. White pigments at shelters I and V are enriched in Ca, P, and S compared to the substrate, suggesting hydroxyapatite and gypsum, while those at shelter II are rich in Si and Al, indicating an aluminosilicate clay mineral base (likely kaolinite-group). The red pigments at Casa Forestal II are distinguished by a modest but consistent increase in Fe (mean 0.64%) compared to the rock (0.35%) and the whites (mean 0.35%), supporting the hypothesis of hematite addition to the base clay recipe.

These interpretations align with and extend earlier chemical analyses of Albarracín rock art. As Beltrán Martínez [41] noted in 1968: "The chemical analyses conducted to date have only allowed us to verify the extreme degree of fossilization of the pigments and to determine the presence of iron, aluminum, and manganese. These consist of ochres and manganese and iron oxides, plus kaolin for white, in addition to hematite, limonite, sanguine, and charcoal" [tr.]. Our pXRF analyses confirm and substantially expand upon these early observations, providing quantitative data that reveals the complexity and variability of pigment recipes across the Albarracín shelters, while also identifying materials not previously reported, such as phosphate-based compounds from bone processing.

4.2. Universal and Pigment-Specific Discriminating Elements

The dominance of substrate-derived elements in multivariate discrimination must be interpreted carefully in an archeological context. The 92.6%–100% classification accuracies achieved by LDA reflect the strength of geological signatures, not necessarily the fidelity of pigment recipe reconstruction. In fact, the largest effect sizes (Cohen's $d > 8.0$) invariably correspond to substrate-driven elements (Ba, Sr-Si-Mg), while elements with unambiguous pigment origins (Fe in reds, Mn in blacks where strongly elevated above substrate, P in suspected bone-char materials) show somewhat smaller but still very large effects ($d = 2.87–7.50$). This hierarchical pattern demonstrates that site discrimination is primarily a geological phenomenon enabling provenance fingerprinting and authentication of painted surfaces, while archaeological interpretation of technological choices must focus on secondary signals—elements clearly enriched in pigments over substrate, and compositional heterogeneity within shelters reflecting multiple painting episodes, diverse raw material sources, or varied preparation techniques.

Barium emerges as the sole element with universal discriminatory power across all pigment types, ranking as the top or second discriminator in each dataset (Tables S9, S17 and S25). Its consistently extreme effect sizes in pairwise comparisons (the largest observed for any element) align with regional geological variations in the Hercynian materials of the Iberian Range [42]. This pattern indicates that Ba primarily reflects substrate-derived signals rather than intentional additions, as confirmed by comparable concentrations in unpainted rock surfaces (Table S2).

The dominance of Ba as a discriminator in the Albarracín sandstone substrates contrasts markedly with Levantine rock art sites on calcareous supports, where Roldán García et al. [18] reported calcium as the overwhelmingly dominant element in all EDXRF spectra from Saltadora (Valltorta gorge, Castellón) due to the limestone bedrock contribution. In that limestone environment, the calcium signal from the substrate complicated pigment-substrate discrimination and required trace element analysis (Mn, As, Pb) to differentiate between pigment sources. At Albarracín, the relatively low calcium concentrations combined with the sandstone matrix allow barium's more subtle geological variations to emerge as the primary discriminator—a pattern that would be masked in calcareous environments.

Other discriminators are markedly pigment-specific, reflecting chromophore selection and preparation. For red pigments, Fe dominates discrimination (Table S25), with raw concentrations confirming hematite (α-Fe_2O_3)/goethite (Fe(OH)O) as the principal

chromophore, consistent with identifications in prior studies of Levantine art [11,43]. The substantial inter-shelter Fe variation—Tío Campano showing approximately three-fold higher mean Fe than Casa Forestal II (Table S26)—suggests exploitation of different ochre sources with varying iron oxide content. The two red pigment samples falling outside standard classification—Hoya de Navarejos III (sample 19) and Cocinilla del Obispo (sample 78)—merit interpretive consideration despite their borderline outlier status. Sample 19 corresponds to a light-toned, pinkish (rather than red) depiction, with the compositional difference likely resulting from varied pigment load or density compared to other motifs on the same panel (Hoya de Navarejos III 20–25). The dimensions, execution technique, and morphology all indicate synchronous creation during a single stylistic phase, as confirmed by consistent readings from other sampling points on the same figure. In contrast, Cocinilla del Obispo 78 exhibits both coloration and morphological differences from other zoomorphic motifs in its shelter, strongly suggesting a distinct pigment composition derived from an alternate raw material source. These cases illustrate how statistical outliers can reflect genuine technological variability—whether through intentional recipe modification within a single painting episode or exploitation of different ochre deposits.

The Tío Campano samples, while not formal outliers, warrant specific discussion due to their distinctive characteristics. All three samples share strong internal compositional similarity despite originating from different figures, supporting synchronous panel execution. Their emergence as a well-defined cluster completely separate from other red pigments underscores both their tonal and stylistic distinctiveness within the Sierra de Albarracín corpus. These figures diverge substantially from the more common formal criteria of regional zoomorphic depictions, exhibiting a non-naturalistic stylistic tendency that suggests exclusion from the Levantine tradition *sensu stricto*. The chemical homogeneity within this atypical stylistic group demonstrates that compositional clustering can successfully identify culturally or chronologically distinct painting episodes, even when visual assessment alone might prove ambiguous.

Manganese distinguishes black pigments (Table S17), but its distribution reveals technological heterogeneity both between and within shelters. Elevated Mn in specific samples (exceeding 0.5% and reaching >2% in some cases; Table S1) indicates pyrolusite use, while Mn-absent or trace-level samples from the same shelters and across Hoya de Navarejos IV, Cabras Blancas, and Prado Navazo suggest carbon-based alternatives (see Section 4.3).

White pigments generally lack a clear chromophore discriminator, instead relying on the Sr-Si-Mg triad (Table S9), which exhibits identical statistical behavior across analyses—a hallmark of covariant substrate, suggesting minerals like celestite ($SrSO_4$) and dolomite/teruelite ($CaMg(CO_3)_2$) in the local sandstones (Table S2).

Secondary patterns include the Zr-P-S triad in black pigments (Table S17), potentially tracing apatite or zircon accessories, and ubiquitous S and Cl across all samples, including substrates (Tables S1 and S2). The sulfur distribution shows site-specific patterns: at Ceja de Piezarrodilla, elevated S values in pigments align with high substrate levels, indicating geological origin. Conversely, at La Cocinilla del Obispo, anomalously high S in specific pigment samples against a low substrate background suggests Liesegang banding—periodic precipitation patterns concentrating sulfates such as gypsum ($CaSO_4 \cdot 2H_2O$) in localized zones. Chlorine, showing more uniform distribution, likely derives from atmospheric deposition of Ebro Valley aerosols, as documented in regional geochemical surveys [44].

4.3. Shelter-Specific Signatures and Cross-Color Consistencies

Pairwise Euclidean distances (Tables S8, S16 and S24) and HCA reveal shelter clusters that vary by pigment color, indicating that geological signatures are modulated by an-

thropogenic choices. Four shelters provided sufficient samples ($n \geq 3$) for multiple colors, enabling cross-color comparisons: Ceja de Piezarrodilla, Hoya de Navarejos III, and Prado Navazo (white and black/black-over-white); Casa Forestal II (white and red).

Ceja de Piezarrodilla emerges as the most chemically complex shelter, exhibiting the highest diversity across white (Table 2) and black (Table 5) pigments. The shelter contains: high-Mn blacks indicating pyrolusite use, moderate-Mn layered samples, and Mn-absent blacks suggesting carbon-based alternatives—all coexisting within a single decorated panel. This heterogeneity—reflected in lower LDA accuracy (62.5% for white)—persists despite proximity to Hoya de Navarejos II and IV (distances 2.76 and 3.85, respectively), suggesting either localized substrate variability or multiple painting phases with different technologies.

The interpretation of white pigment outliers at this shelter merits particular attention. Sample 1, located at a contact zone between different chromatic elements, likely reflects a combined signal from white horns and overlying black repaint, explaining its distinct cluster identity. More intriguing is sample 5, corresponding to white horns, which shows the closest compositional similarity to a stylized human representation from Hoya de Navarejos II rather than to other white bovine figures with twisted-perspective horns (such as those from Hoya de Navarejos III or Prado del Navazo). These evident thematic and morphological differences—despite chemical correspondence—suggest that pigment recipes were not strictly determined by subject matter or style, but may reflect the use of different geological raw material sources even among morpho-stylistically similar representations.

Hoya de Navarejos III shows moderate consistency across colors (Tables S8 and S16), yet exhibits the same internal technological heterogeneity as Ceja de Piezarrodilla—the shelter contains the highest single Mn value in a black pigment and Mn-free black samples (Table S1), documenting deliberate material choices rather than simple substrate influence. Casa Forestal II displays color-dependent divergence: tight clustering for white (single cluster) but moderate diversity in red, with Fe levels that contrast markedly with Tío Campano's, implying distinct ochre sources.

The black-over-white and white-over-black samples, concentrated in Ceja de Piezarrodilla (n = 5) and Cabras Blancas (n = 11), show distinct patterns. Ceja de Piezarrodilla black-over-white samples contain moderate Mn, suggesting Mn-based black pigment beneath the white overlayer. In contrast, Cabras Blancas white-over-black samples show negligible Mn and P, indicating different black pigment technology or more complete coverage by the white overlayer.

Overall, PERMANOVA confirms location as the primary variance driver (Tables 3, 6 and 9), explaining 49%–68% of compositional differences—values indicative of strong geological control tempered by pigment type and technological choices.

4.4. Insights into Pigment Technology and Raw Material Procurement

The pigment-specific discriminators illuminate prehistoric technological repertoires with unexpected complexity. Red pigments uniformly implicate Fe-rich ochres, but substantial inter-shelter Fe variation (Table S26) suggests exploitation of diverse sources, possibly from local ferricretes, as inferred from similar variability in Cantabrian rock art [45]. The absence of correlated As or Hg (Table S1) excludes the use of iron arsenopirite or cinnabar admixtures.

Black pigments reveal a dual technology that transcends shelter boundaries: Mn-oxide-based pigments occur at Ceja de Piezarrodilla, Hoya de Navarejos III, and La Cocinilla del Obispo, versus Mn-absent alternatives found at Hoya de Navarejos IV, Cabras Blancas, Prado Navazo, and remarkably, within the same shelters showing Mn-rich samples (Hoya de Navarejos III and Ceja de Piezarrodilla, Table S1). This within-shelter coexistence of Mn-rich and Mn-poor blacks represents the clearest evidence for technological diversity.

The P association in low-Mn samples, when exceeding substrate baselines (Table S2), is consistent with bone-derived materials, as P would derive from hydroxyapatite in calcined bone [46]. However, the identification of bone char based on phosphorus enrichment alone requires explicit consideration of alternative P sources. Substrate-derived phosphorus from accessory apatite minerals in the sandstones cannot be entirely excluded, though the selective enrichment in specific pigment samples rather than uniform distribution argues against substrate as the primary source. Post-depositional contamination from guano represents another possibility, though sampling avoided visibly contaminated areas, and the spatial pattern (P elevation in specific motifs rather than diffuse across panels) favors original pigment composition. Diagenetic phosphorus mobilization from organic matter decomposition typically produces diffuse enrichment rather than the localized patterns observed here.

On balance, the bone-derived materials hypothesis remains the most parsimonious interpretation given: (1) clear P enrichment above substrate baselines, (2) co-enrichment with Ca consistent with hydroxyapatite, (3) ethnographic parallels documenting bone char use in prehistoric contexts, and (4) the functional association with Mn-poor blacks (substitution where manganese oxides are unavailable). Nevertheless, definitive confirmation requires complementary techniques—Raman spectroscopy to identify carbon species and distinguish bone char from vegetal charcoal, or SEM-EDS to detect bone microstructure. Pending such analyses, P-enriched pigments are interpreted as "consistent with possible bone-derived materials" rather than confirmed bone char.

The technological duality within Ceja de Piezarrodilla—encompassing high-Mn mineral blacks, low-Mn carbon-based pigments (possibly including bone char), and the anomalous high-Mn white—indicates either episodic use of different recipes or complex stratigraphic relationships.

This dual black pigment technology parallels findings by Roldán García et al. [18] at Saltadora (Valltorta gorge, Castellón), where EDXRF analysis on calcareous substrates identified manganese oxides with barium as a trace element in black deer figures, with Mn-Ba correlation suggesting romanechite or hollandite minerals. However, subsequent work at Cova Remigia [25] and Cingle de la Mola Remigia [47] identified carbon-based blacks via Raman spectroscopy—charcoal without detectable phosphorus or manganese via EDXRF. The phosphorus enrichment we document in low-Mn blacks at Albarracín is consistent with bone char rather than simple charcoal, potentially representing a third black pigment technology within the Levantine tradition. The fundamental substrate difference (sandstone at Albarracín vs. limestone at Saltadora/Cova Remigia, where calcium dominates all EDXRF spectra) explains why our discrimination patterns differ from those coastal sites.

The exceptional white pigment with 2.108% Mn (Ceja de Piezarrodilla sample 1) warrants special consideration. Possible explanations include sampling of a palimpsest where white was applied over manganese-rich black, with pXRF penetrating both layers, or diagenetic Mn precipitation forming dendrites or coatings subsequently covered by white pigment. The co-occurrence with P (1.010%) suggests a possible association with organic materials.

White pigments generally derive from substrate-like materials, likely aluminosilicate clay minerals or calcitic components (high Al-Si), with no evidence of exotic additives (e.g., Sn, Sb < LOD). The Sr-Si-Mg triad's perfect covariance confirms natural geological origin rather than deliberate mixing.

4.5. Methodological Considerations, Limitations, and Future Directions

The multivariate pXRF analysis of 102 pigment samples from 11 shelters in the Albarracín Cultural Park reveals systematic geochemical patterns that reflect the complex interplay between substrate geology, pigment composition, and post-depositional processes. While the penetration depth of pXRF (typically 1–5 mm for major elements in siliceous matrices) captures a composite signal from both the thin pigment layer (often <50 μm) and the underlying rock substrate, the resulting datasets enable robust discrimination among shelters and provide unexpected insights into prehistoric technological choices. The centered log-ratio (CLR) transformation and subsequent multivariate analyses (PCA, LDA, HCA) consistently demonstrate large between-shelter variances, with effect sizes (Tables S9, S17 and S25) that far exceed those typically reported in archaeometric studies of rock art [48,49]. The correlation between effect size magnitude and element type—with substrate-derived elements showing the most extreme values—confirms that geological variation drives much of the observed discrimination, though pigment-specific patterns remain detectable as secondary signals.

The CLR approach effectively mitigated compositional constraints, revealing covariant groups (e.g., Sr-Si-Mg) that standard analyses might misattribute. However, the composite signals limit pure recipe reconstruction; future synchrotron μ-XRF or LA-ICP-MS could isolate surface layers [50]. Small sample sizes for some shelter-color combinations (e.g., $n = 1$ for Hoya de Navarejos V white, La Cocinilla del Obispo black) constrain generalizability, though bootstrap validation (94.1–100.0% accuracy) affirms robustness for adequately sampled locations.

For heritage management, the 92.6%–100% LDA accuracies enable fingerprinting for authentication, particularly valuable for UNESCO-listed Levantine art vulnerable to looting. High diversity at Ceja de Piezarrodilla flags this shelter for priority investigation regarding differential deterioration risks. The variable sulfur distributions—from substrate-derived to localized diagenetic enrichments via Liesegang banding (Tables S1 and S2)—combined with widespread chlorine presence from atmospheric deposition, underscore the complex deterioration pathways affecting these paintings. While Cl contamination warrants atmospheric monitoring amid climate-driven increases in Saharan dust transport to Iberia [51], the site-specific sulfur patterns require targeted conservation strategies. These findings advocate integrated geoarchaeometric protocols for prioritizing interventions in similar open-air sites [52].

The case of Ceja de Piezarrodilla's black pigment samples 14 and 15 illustrates how differential preservation can generate statistically significant compositional outliers. These samples, from the bovine's hindquarters, represent the only portion unaffected by whitish biofilm that has progressively covered the figure's anterior section [9]. Their chemical distinctiveness likely reflects the purest signal of original pigment composition, while anterior samples yield composite signals from pigment, substrate, and biological overgrowth. This demonstrates that 'outliers' in rock art pXRF datasets may paradoxically preserve the most faithful record of original technological choices, with 'typical' samples potentially representing degraded or contaminated states. Such preservation-driven chemical variation underscores the importance of integrating taphonomic assessment with geochemical analysis when interpreting compositional patterns.

Several methodological limitations constrain the interpretive scope of this study. First, pXRF provides elemental composition but cannot identify mineral phases; all mineral identifications (pyrolusite, hematite, gypsum, kaolinite-group clays, hydroxyapatite) remain provisional hypotheses based on characteristic elemental associations rather than definitive structural identification. Portable X-ray diffraction (pXRD) would provide the necessary phase identification to validate or refute these interpretations. Second, the composite signal

geometry limits recipe reconstruction; while elements clearly enriched above substrate baselines document genuine technological choices, the absolute proportions of pigment versus substrate contributions remain uncertain. Surface-sensitive techniques (confocal Raman microscopy, synchrotron μ-XRF) could provide layer-resolved analysis. Third, the absence of quantitative colorimetry precludes statistical correlation between elemental composition and visual color properties; future studies incorporating spectrophotometric L*a*b* measurements could establish whether subtle compositional variations correlate with perceptible hue differences within color categories. Fourth, carbon-based pigments (charcoal, bone char) are invisible to XRF; Raman spectroscopy is required to identify carbon species and distinguish vegetal charcoal from bone char based on characteristic spectral features. Fifth, small sample sizes for some shelter-color combinations limit the generalizability of conclusions for those specific groups. Sixth, the substrate characterization (n = 9 measurements per shelter) provides representative rather than exhaustive coverage; localized substrate heterogeneity within shelters may contribute additional variance not captured by our sampling design.

These limitations notwithstanding, the systematic patterns documented here provide a robust foundation for targeted follow-up studies. Future research directions include: (1) pXRD for definitive mineral phase identification; (2) Raman spectroscopy for carbon speciation and organic binder identification; (3) quantitative colorimetry combined with elemental/mineralogical data; (4) where conservation permits, targeted micro-sampling for surface-sensitive laboratory techniques providing layer-resolved analysis.

4.6. Implications for Understanding Prehistoric Painting Practices

The extraordinary effect sizes observed (Tables S11, S19 and S27) represent some of the largest reported in archeological chemistry, indicating that between-shelter variance overwhelmingly dominates within-shelter variance. While this enables excellent site discrimination, it simultaneously suggests that geological overprinting may partially obscure anthropogenic signals. The relationship between effect size and element type provides insight: substrate-derived elements (Ba, Sr-Si-Mg group) yield the most extreme values, while elements clearly associated with intentional pigment use (Fe in red, Mn in black, where intentionally added) show large but less extreme effects.

The technological complexity revealed (particularly the dual black pigment technologies at Ceja de Piezarrodilla and Hoya de Navarejos III) suggests more sophisticated painting practices than previously recognized. The coexistence of manganese-based and carbon-based black pigments within single shelters may reflect diachronic changes in raw material availability or cultural preferences, or work by different artist groups with distinct technological traditions. The black-over-white samples further indicate deliberate layering strategies, though the chemical penetration of pXRF complicates interpretation of intentionality versus superimposition.

The persistence of shelter-specific signatures across different pigment colors, exemplified by Ceja de Piezarrodilla's consistent heterogeneity and the Casa Forestal complex's relative homogeneity, confirms that local geology exerts primary control on chemical profiles. However, the documented technological choices (selective use of manganese oxides versus carbon-based materials, variable iron oxide sources, and complex layering) demonstrate that cultural factors significantly modulate these geological baselines.

The compositional heterogeneity observed within individual shelters carries significant archeological implications. At Ceja de Piezarrodilla, the coexistence of Mn-rich black pigments (samples 2, 3, 6: >0.33% Mn) and Mn-poor alternatives (samples 14, 15: <0.2% Mn) within the same decorated panel indicates either: (1) multiple episodic painting events with evolving material preferences over time, (2) parallel workshop traditions with distinct

technological knowledge operating contemporaneously, or (3) functional differentiation of pigment types for specific applications. The similar pattern at Hoya de Navarejos III reinforces this interpretation. Conversely, the relative homogeneity at Casa Forestal suggests a more coordinated raw material procurement strategy, possibly reflecting single painting episodes or standardized workshop practices.

The specific enrichment patterns documented (Fe in reds exceeding substrate baselines by factors of 1.5–6×, Mn in specific blacks reaching concentrations 10–20× above detection limits where substrate Mn is consistently <LOD) cannot be attributed to layer thickness variations alone and document genuine technological choices. These findings challenge assumptions about technological homogeneity in Levantine art production and indicate that Albarracín rock art represents sophisticated technological systems rather than opportunistic use of immediately available materials.

5. Conclusions

This pXRF analysis of 102 pigment samples from 12 rock art shelters in the Albarracín Cultural Park demonstrates that multivariate statistical approaches can successfully discriminate between archeological sites despite the composite signals inherent in portable XRF measurements. The application of centered log-ratio transformation effectively addressed compositional data constraints, achieving classification accuracies of 92.6%–100% through linear discriminant analysis.

Barium emerged as a consistent discriminator across all pigment types, primarily reflecting regional geological variations rather than intentional additions. Pigment-specific patterns revealed distinct technological choices: iron-rich compositions consistent with ochre/hematite in red pigments; manganese distributions documented dual technologies for black pigments, with both manganese oxide and carbon-based materials (possibly including bone char based on phosphorus enrichment) employed sometimes within the same shelter; and white pigments showed combinations of substrate-derived materials with gypsum and kaolinitic clays, occasionally incorporating hydroxyapatite.

The large effect sizes observed (Cohen's d up to 9.19) primarily reflect the methodological characteristics of pXRF, which captures integrated signals from both thin pigment layers and underlying substrates. This substrate dominance, while enabling robust site discrimination, limits direct reconstruction of pigment recipes. Nevertheless, elements showing clear enrichment above substrate baselines document genuine technological choices: iron for red ochres, manganese for specific black pigments, and phosphorus in materials consistent with possible bone-derived components. The within-shelter heterogeneity documented at Ceja de Piezarrodilla and Hoya de Navarejos III (where chemically distinct pigment recipes coexist) indicates multiple painting episodes, diverse procurement strategies, or parallel technological traditions rather than homogeneous painting practices.

Future research directions to address the limitations of pXRF-only analysis include: (1) portable X-ray diffraction (pXRD) for definitive mineral phase identification, resolving ambiguities in clay mineral, iron oxide, and manganese oxide species; (2) Raman spectroscopy for carbon speciation, distinguishing bone char from vegetal charcoal and identifying organic binders; (3) quantitative colorimetry (CIE L*a*b*) combined with elemental data to establish relationships between pigment composition and visual color properties; and (4) where conservation permits, targeted micro-sampling for surface-sensitive laboratory techniques providing layer-resolved analysis. The combination of pXRF screening (coverage and statistical power demonstrated here) with surface-sensitive complementary techniques represents the optimal analytical strategy for comprehensive rock art characterization.

For heritage management, the site-specific chemical fingerprints provide a tool for authentication and provenance determination. The identification of variable sulfur distributions and ubiquitous chlorine contamination highlights ongoing deterioration processes requiring targeted conservation strategies. The chemical heterogeneity documented at sites like Ceja de Piezarrodilla and Hoya de Navarejos III, where both manganese-based and carbon-based black pigments coexist, suggests complex painting histories that warrant detailed investigation. These findings establish a quantitative baseline for monitoring the preservation state of these UNESCO World Heritage sites while revealing greater technological diversity in Levantine rock art production than previously recognized.

Supplementary Materials: The following supporting information can be downloaded at: https://www.mdpi.com/article/10.3390/min15121328/s1, Figures S1–S12: Original pictures and digital tracings of analyzed paintings from Cabras Blancas, Casa Forestal I, Casa Forestal II, Casa Forestal V, Ceja de Piezarrodilla, Hoya de Navarejos II, Hoya de Navarejos III, Hoya de Navarejos IV, Hoya de Navarejos V, La Cocinilla del Obispo, Prado Navazo, and Tío Campano shelters showing sampling points [8,10,13,27,30,53–55]; Table S1: Raw elemental composition data for all pigment samples (all elements detected); Table S2: Elemental composition of unpainted rock substrates by shelter; Table S3: Z-scores of CLR-transformed data for 15 compositional variables (all samples); Table S4: Principal component analysis results for white pigment samples (n = 54); Table S5: Factor loadings from the principal component analysis of white pigment samples; Table S6: Sequential tests of discriminant functions for white pigments samples; Table S7: Structure matrix—correlations between elements and discriminant functions for white pigment samples; Table S8: Pairwise Euclidean distance matrix between white pigment sampling locations based on mean elemental compositions (n = 54 samples, 9 locations); Table S9: Statistical summary for the most discriminating elements in white pigment samples; Table S10: Mean Z-scores and standard deviations for the most discriminating elements in white pigment samples, organized by location; Table S11: Complete Cohen's d values for pairwise comparisons—white pigments; Table S12: Principal component analysis results for black, black-over-white, and white-over-black pigment samples (n = 31); Table S13: Factor loadings from the principal component analysis of black, black-over-white, and white-over-black pigments; Table S14: Sequential tests of discriminant functions for black, black-over-white, and white-over-black pigment samples; Table S15: Structure matrix—correlations between elements and discriminant functions for black, black-over-white, and white-over-black pigment samples; Table S16: Pairwise Euclidean distance matrix between black, black-over-white, and white-over-black pigment sampling locations based on mean elemental compositions (n = 31 samples, 6 locations); Table S17: Statistical summary for the five most discriminating elements in black, black-over-white, and white-over-black pigment samples; Table S18: Mean Z-scores and standard deviations for the five most discriminating individual elements in the black, black-over-white, and white-over-black pigment samples, organized by location; Table S19: Complete Cohen's d values for pairwise comparisons—black, black-over-white, and white-over-black pigments; Table S20: Principal component analysis results for red pigment samples (n = 17); Table S21: Factor loadings from the principal component analysis of red pigment samples; Table S22: Sequential tests of discriminant functions for red pigment samples; Table S23: Structure matrix—correlations between elements and discriminant functions for red pigment samples; Table S24: Pairwise Euclidean distance matrix between red pigment sampling locations based on mean elemental compositions (n = 17 samples, 5 locations); Table S25: Statistical summary for the most discriminating elements in the red pigment samples; Table S26: Mean Z-scores and standard deviations for the most discriminating elements in red pigment samples, organized by location; Table S27: Complete Cohen's d values for pairwise comparisons—red pigments.

Author Contributions: Conceptualization, M.B.-M. and J.A.C.-O.; methodology, P.M.-R.; software, P.M.-R.; validation, J.A.C.-O.; formal analysis, P.M.-R. and J.A.C.-O.; investigation, P.M.-R., J.A.C.-O. and M.B.-M.; resources, M.B.-M.; data curation, P.M.-R.; writing—original draft preparation, P.M.-R., J.A.C.-O. and M.B.-M.; writing—review and editing, P.M.-R., J.A.C.-O. and M.B.-M.; visualization,

P.M.-R. and M.B.-M.; project administration, M.B.-M.; funding acquisition, M.B.-M. All authors have read and agreed to the published version of the manuscript.

Funding: This research was funded by the Dirección General de Ciencia e Innovación of the Gobierno de Aragón, under the project 'Searching for the Origins of Rock Art in Aragón (SEFORA)', grant number PROY_H04_24.

Data Availability Statement: All of the data supporting the findings of this study are available within the paper and its Supplementary Information. Should any raw data files be needed in another format, they are available from the corresponding author upon reasonable request.

Acknowledgments: The authors gratefully acknowledge the support of Hilario Dalda Abril, Agent for the Protection of Cultural Heritage of the Government of Aragon. During the preparation of this manuscript, the authors used Claude Sonnet 4.5 in order to improve the readability and language of the manuscript. The authors have reviewed and edited the output and take full responsibility for the content of this publication.

Conflicts of Interest: The authors declare no conflicts of interest. The funders had no role in the design of the study; in the collection, analyses, or interpretation of data; in the writing of the manuscript; or in the decision to publish the results.

Abbreviations

The following abbreviations are used in this manuscript:

ANOVA	Analysis of Variance
ARAMPI	Rock Art of the Mediterranean Basin on the Iberian Peninsula
BDL	Below Detection Limit
CI	Confidence Interval
CLR	Centered Log-Ratio
HCA	Hierarchical Cluster Analysis
LDA	Linear Discriminant Analysis
MANOVA	Multivariate Analysis of Variance
PCA	Principal Components Analysis
PERMANOVA	Permutational Multivariate Analysis of Variance
pXRF	portable X-ray fluorescence
SEM-EDX	Scanning Electron Microscopy-Energy Dispersive X-ray
UNESCO	United Nations Educational, Scientific, and Cultural Organization

References

1. Siddall, R. Mineral pigments in Archaeology: Their analysis and the range of available materials. *Minerals* **2018**, *8*, 201. [CrossRef]
2. Sepúlveda, M. Making visible the invisible. A microarchaeology approach and an Archaeology of Color perspective for rock art paintings from the southern cone of South America. *Quat. Int.* **2021**, *572*, 5–23. [CrossRef]
3. Pollard, A.M.; Batt, C.M.; Stern, B.; Young, S.M.M. *Analytical Chemistry in Archaeology*; Cambridge University Press: Cambridge, UK; New York, NY, USA, 2007; p. 404. [CrossRef]
4. Madariaga, J.M. Analytical chemistry in the field of cultural heritage. *Anal. Methods* **2015**, *7*, 4848–4876. [CrossRef]
5. Hernanz, A.; Gavira-Vallejo, J.M. Rock Art. In *Analytical Strategies for Cultural Heritage Materials and Their Degradation*; Madariaga, J.M., Ed.; The Royal Society of Chemistry: London, UK, 2021; pp. 201–226. [CrossRef]
6. Marconell, E. Los toros de la Losilla. *Rev. Miscelánea Turol.* **1892**, *9*, 160.
7. Marconell, E. Los toros de la Losilla. *Rev. Miscelánea Turol.* **1892**, *10*, 180.
8. Piñón Varela, F. *Las Pinturas Rupestres de Albarracín (Teruel)*; Dirección General de Bellas Artes, Archivos y Bibliotecas: Santander, Spain, 1982; Volume 6.
9. Bea Martínez, M.; Angás Pajas, J. Las representaciones levantinas de bovinos de la Casa Forestal de Tormón (Teruel): Ceja de Piezarrodilla y Cerrada del Tío Jorge. *Zephyrus Rev. De Prehist. Y Arqueol.* **2015**, *75*, 73–84.

10. Bea Martínez, M.; Angás Pajas, J.G.S.; Miguel, L.; Gutiérrez, F.J.; Longares Aladrén, L.A.M.; Salvador; Peña Monné, J.L. *Las Pinturas Rupestres de Bezas Y Tormón (Teruel)*; Bea Martínez, M., Angás Pajas, J., Eds.; Parque Cultural de Albarracín: Teruel, Spain, 2015; p. 182.
11. Orera Clemente, V.M.; Bea Martínez, M.; Domingo, R.; Utrilla, P. Costras de yeso responsables de la degradación de pinturas levantinas en la provincia de Teruel. In Proceedings of the I Simposio anual de Patrimonio Natural y Cultural ICOMOS España, Valencia, Spain, 21–23 November 2019; pp. 569–576. [CrossRef]
12. Bea Martínez, M. Novedades en torno al núcleo rupestre levantino de la Sierra de Albarracín. El abrigo de Prao Medias (Tormón, Teruel). *Saguntum Papeles Lab. Arqueol. Valencia* **2014**, *46*, 203–207. [CrossRef]
13. Bea Martínez, M. El abrigo de Hoya de Navarejos III (Tormón, Teruel). Nuevas perspectivas para el análisis del arte levantino interior. *Complutum* **2017**, *28*, 37–50. [CrossRef]
14. Bea Martínez, M.; Angás Pajas, J. Reestudio de los conjuntos rupestres de Las Tajadas de Bezas (Teruel). *Cuad. Arte Rupestre* **2013**, *6*, 129–145.
15. Bea Martínez, M.; Angás Pajas, J. Planteamientos interpretativos para el arte levantino a partir del estudio del abrigo del Arquero de los Callejones Cerrados. *Zephyrus Rev. Prehist. Y Arqueol.* **2016**, *77*, 59–78.
16. Martínez-Bea, M. Arte rupestre de Albarracín: La excepcionalidad de un conjunto interior. In Proceedings of the IV Congreso del Neolítico Peninsular, Alicante, Spain, 27–30 November 2006; pp. 141–148.
17. Serrano Aranda, C.; Zalbidea Muñoz, A.; Bea Martínez, M. Propuesta de conservación-restauración para el conjunto con arte rupestre Levantino de Los Toros del Prado del Navazo (Albarracín, Teruel, España). *TAREA* **2021**, *8*, 206–240.
18. Roldán García, C.; Murcia-Mascarós, S.; Ferrero, J.; Villaverde, V.; López, E.; Domingo, I.; Martínez, R.; Guillem, P.M. Application of field portable EDXRF spectrometry to analysis of pigments of Levantine rock art. *X-Ray Spectrom.* **2010**, *39*, 243–250. [CrossRef]
19. Mas, M.; Jorge, A.; Gavilán, B.; Solís, M.; Parra, E.; Pérez, P.-P. Minateda rock shelters (Albacete) and post-palaeolithic art of the Mediterranean Basin in Spain: Pigments, surfaces and patinas. *J. Archaeol. Sci.* **2013**, *40*, 4635–4647. [CrossRef]
20. Roldán García, C.; Murcia-Mascarón, S.; Ferrero, J.; Villaverde, V.; Martínez, R.; Guillem, P.; Domingo Sanz, I.; López Montalvo, E. Anexo I: Análisis in situ de pigmentos de las pinturas levantinas de los abrigos VII, VIII y IX de la Saltadora mediante fluorescencia de Rayos-X. In *Los Abrigos VII, VIII y IX de les Coves de la Saltadora. Monografías del Instituto de Arte Rupestre II*; Domingo Sanz, I., López Montalvo, E., Villaverde Bonilla, V., Martínez Valle, R., Eds.; Generalitat Valenciana València: Valencia, Spain, 2007; pp. 192–205.
21. Roldán García, C. Análisis de pigmentos en conjuntos de arte rupestre. In Proceedings of the El arte rupestre del Arco Mediterráneo de la Península Ibérica: 10 años en la lista del Patrimonio Mundial de la UNESCO, Valencia, Spain, 3–5 December 2008; pp. 269–278.
22. Hernanz, A.; Ruiz-López, J.F.; Gavira-Vallejo, J.M.; Martin, S.; Gavrilenko, E. Raman microscopy of prehistoric rock paintings from the Hoz de Vicente, Minglanilla, Cuenca, Spain. *J. Raman Spectrosc.* **2010**, *41*, 1394–1399. [CrossRef]
23. Alloza Izquierdo, R.; Arranz Yagüe, E.; González Grau, J.M.; Baldellou Martínez, V.; Resano, M.; Marzo, P.; Vanhaecke, F. La conservación del arte rupestre: Estudio de los factores de deterioro y de la composición química de los pigmentos. In *El Arte Rupestre del Arco Mediterráneo de la Península Ibérica: 10 Años en la Lista del Patrimonio Mundial de la UNESCO*; Generalitat Valenciana: Valencia, Spain, 2009; pp. 317–326.
24. López-Montalvo, E.; Gallello, G.; Roldán, C.; Ramacciotti, M.; Goemaere, E.; Rubio, A.M.; Murcia-Mascaròs, S.; Subirats, P. New insights into the Spanish Levantine rock art pigments combining pXRF and stylistic approach: The Coco de la Gralla site (Mas de Barberans, Tarragona, Spain) as a case study. *J. Archaeol. Sci. Rep.* **2025**, *66*, 105273. [CrossRef]
25. López-Montalvo, E.; Villaverde, V.; Roldán, C.; Murcia, S.; Badal, E. An approximation to the study of black pigments in Cova Remigia (Castellón, Spain). Technical and cultural assessments of the use of carbon-based black pigments in Spanish Levantine Rock Art. *J. Archaeol. Sci.* **2014**, *52*, 535–545. [CrossRef]
26. Martín-Ramos, P.; Cuchí-Oterino, J.A.; Bea-Martínez, M. Portable X-ray Fluorescence Analysis of Levantine and Schematic Art Pigments from the River Vero Shelters (Huesca, NE Spain). *Heritage* **2023**, *6*, 3789–3800. [CrossRef]
27. Beltrán Martínez, A. *Arte Rupestre Levantino*; Universidad de Zaragoza: Zaragoza, Spain, 1968; Volume IV.
28. Orera Clemente, V.; Bea Martínez, M.; Peña Monné, J.L.; Utrilla Miranda, M.d.P. Análisis de pigmentos del abrigo de Cabras Blancas (Tormón, Teruel). In Proceedings of the III Congreso CAPA Arqueología Patrimonio Aragonés, Zaragoza, Spain, 14–15 November 2019; pp. 73–81.
29. Beltrán Martínez, A. Sobre el arte levantino, especialmente de Albarracín: Ideas generales para un debate. In Proceedings of the Actas del XXI Congreso Nacional de Arqueología, Teruel, Spain, 8–11 October 1991; pp. 289–316.
30. Beltrán Martínez, A. *Arte prehistórico en Aragón*; Ibercaja: Zaragoza, Spain, 1993; p. 228.

31. Hernández, A.; Olivé, A.; Gutiérrez, M.; Aguilar, M.J.; Ramírez, J.; Aragónes, E.; Giner, J.; Riba, O. *Mapa Geológico de España E. 1:50.000—Cella. 566, 26-22*; Instituto Geológico y Minero de España; Servicio de Publicaciones Ministerio de Industria y Energía: Madrid, Spain, 1983; p. 71.
32. Aznar, J.M.; Olivé, A.; Moissenet, E.; Hernández, A.; Portero, J.M.; Gutiérrez, M.; Aguilar, M.J.; Ramírez, J.; Aragónes, E.; Giner, J. *Mapa Geológico de España E. 1:50.000—Terriente. 589, 26-23*; Instituto Geológico y Minero de España. Servicio de Publicaciones Ministerio de Industria y Energía: Madrid, Spain, 1983; p. 83.
33. De la Cruz, B.; Marfil Pérez, R.; De la Peña, J.; Arribas Mocoroa, J. Procedencia y evolución diagenética de las areniscas permo-triásicas de la Cordillera Ibérica (Sierra de Albarracin-Boniches-Talayuelas, provincias de Teruel y Cuenca). *Cuad. De Geol. Ibérica* **1987**, *11*, 493–514.
34. Riba Arderiu, O. *Estudio Geológico de la Sierra de Albarracín*; CSIC (Consejo Superior de Investigaciones Científicas): Madrid, Spain, 1959; Volume 16, p. 283.
35. Pérez-Arlucea, M. Distribución paleogeográfica de las unidades del Pérmico y del Triásico en el sector Molina de Aragón-Albarracín. *Cuad. Geol. Ibérica* **1987**, *11*, 607–622.
36. Pérez-Arlucea, M.; Sopeña, A. Estratigrafía del Pérmico y Triásico en el sector central de la Rama Castellana de la Cordillera Ibérica (provincias de Guadalajara y Teruel). *Estud. Geológicos* **1983**, *41*, 207–222. [CrossRef]
37. Pérez-Arlucea, M.; Sopeña, A. Estudio sedimentológico del Saxoniense y del Buntsandstein entre Molina de Aragón y Albarracín. *Cuad. Geol. Ibérica* **1986**, *10*, 117–150.
38. Sancho Marcén, C.; Benito Ferrández, G.; Machado, M.J. El modelado en areniscas del Ródeno de Albarracín. In *Las Formas del Relieve de la Sierra de Albarracín*; Peña Monné, J.L., Sánchez Fabre, M., Lozano Tena, M.V., Eds.; Centro de Estudios de la Comunidad de Albarracín: Tramacastilla, Teruel, Spain, 2010; pp. 191–217.
39. Benito, G.; Machado, M.J.; Sancho, C. Sandstone weathering processes damaging prehistoric rock paintings at the Albarracin Cultural Park, NE Spain. *Environ. Geol.* **1993**, *22*, 71–79. [CrossRef]
40. Martín-Fernández, J.A.; Barceló-Vidal, C.; Pawlowsky-Glahn, V. Dealing with zeros and missing values in compositional data sets using nonparametric imputation. *Math. Geol.* **2003**, *35*, 253–278. [CrossRef]
41. Beltrán Martínez, A. El arte Rupestre Levantino: Cronología y Significación. *Caesaraugusta* **1968**, *31–32*, 7–43.
42. Osácar Soriano, M.C.; González Martínez, J.; Besteiro Rafales, J. Geoquímica de las mineralizaciones de Baritina de la Unidad de Herrera (Cordillera Ibérica Oriental). *Boletín De La Soc. Española De Mineral.* **1992**, *15*, 157–160.
43. Roldán García, C.; Villaverde Bonilla, V.; Ródenas Marín, I.; Murcia Mascarós, S. A unique collection of Palaeolithic painted portable art: Characterization of red and yellow pigments from the Parpalló Cave (Spain). *PLoS ONE* **2016**, *11*, e0163565. [CrossRef]
44. Querol, X.; Viana, M.; Alastuey, A.; Amato, F.; Moreno, T.; Castillo, S.; Pey, J.; de la Rosa, J.; Sánchez de la Campa, A.; Artíñano, B.; et al. Source origin of trace elements in PM from regional background, urban and industrial sites of Spain. *Atmos. Environ.* **2007**, *41*, 7219–7231. [CrossRef]
45. Iriarte, E.; Foyo, A.; Sánchez, M.A.; Tomillo, C.; Setién, J. The origin and geochemical characterization of red ochres from the Tito Bustillo and Monte Castillo caves (Northern Spain)*. *Archaeometry* **2009**, *51*, 231–251. [CrossRef]
46. Shahack-Gross, R.; Bar-Yosef, O.; Weiner, S. Black-coloured bones in Hayonim Cave, Israel: Differentiating between burning and oxide staining. *J. Archaeol. Sci.* **1997**, *24*, 439–446. [CrossRef]
47. Roldán, C.; Villaverde, V.; Rodenas, I.; López-Montalvo, E.; Domingo Sanz, I.; Murcia, S.; Martínez Valle, R.; Calatayud, P.M. Análisis de pigmentos parietales de Arte Levantino de los abrigos del "Cingle de la Mola Remigia" (Barranco de la Gasulla, Castellón). In Proceedings of the X Congreso Ibérico de Arqueometría, Castellón, Spain, 16–18 October 2013; pp. 128–139. [CrossRef]
48. Chalmin, E.; Menu, M.; Vignaud, C. Analysis of rock art painting and technology of Palaeolithic painters. *Meas. Sci. Technol.* **2003**, *14*, 1590–1597. [CrossRef]
49. Shugar, A.N. Portable X-ray fluorescence and archaeology: Limitations of the instrument and suggested methods to achieve desired results. In *Archaeological Chemistry VIII*; Armitage, R.A., Burton, J.H., Eds.; American Chemical Society: Washington DC, USA, 2013; pp. 173–193. [CrossRef]
50. Chalmin, E.; Huntley, J. Characterizing rock art pigments. In *The Oxford Handbook of the Archaeology and Anthropology of Rock Art*; David, B., McNiven, I.J., Eds.; Oxford University Press: Oxford, UK, 2017. [CrossRef]
51. Prospero, J.M.; Lamb, P.J. African droughts and dust transport to the Caribbean: Climate change implications. *Science* **2003**, *302*, 1024–1027. [CrossRef]
52. Sánchez-Moral, S.; Soler, V.; Cañaveras, J.C.; Sanz-Rubio, E.; Van Grieken, R.; Gysels, K. Inorganic deterioration affecting the Altamira Cave, N Spain: Quantitative approach to wall-corrosion (solutional etching) processes induced by visitors. *Sci. Total Environ.* **1999**, *243–244*, 67–84. [CrossRef]

53. Obermaier, H. Nuevas pinturas rupestres descubiertas en los alrededores de Tormón (Teruel). *Investig. Y Prog.* **1927**, *I*, 1–2.
54. Obermaier, H.; Breuil, H. Las pinturas rupestres de los alrededores de Tormón (Teruel). *Boletín Real Acad. Hist.* **1927**, *90*, 511–531.
55. Piñón Varela, F. Superposiciones y repintados en la serranía de Albarracín: Elementos para el establecimiento de una cronología relativa. In *Altamira Symposium*; Ministerio de Cultura, Dirección General de Archivos, Bibliotecas y Museos: Madrid, Spain, 1981; pp. 411–426.